aerospace

MDPI

Article

An Efficient and Robust Sizing Method for eVTOL Aircraft Configurations in Conceptual Design

Osita Ugwueze [1], Thomas Statheros [1], Nadjim Horri [2], Michael A. Bromfield [3] and Jules Simo [4,*]

[1] Centre for Future Transport and Cities, Coventry University, Coventry CV1 2TE, UK
[2] School of Mechanical, Aerospace and Automotive Engineering, Faculty of Engineering, Environment & Computing, Coventry University, Coventry CV1 5FB, UK
[3] School of Metallurgy and Materials, University of Birmingham, Birmingham B15 2TT, UK
[4] School of Engineering, University of Central Lancashire, Preston PR1 2HE, UK
* Correspondence: jsimo@uclan.ac.uk; Tel.: +44-(0)1772-893545

Abstract: This paper presents the development of a robust sizing method to efficiently estimate and compare key performance parameters in the conceptual design stage for the two main classes of fully electric vertical take-off and landing (eVTOL) aircraft, the powered lift and wingless aircraft types. The paper investigates hybrids of classical root-finding methods: the bisection, fixed-point and Newton-Rapson methods for use in eVTOL aircraft sizing. The improved convergence efficiency of the hybrid methods is at least 70% faster than the standard methods. This improved efficiency is significant for complex sizing problems. The developed sizing method is used to investigate the comparative performance of the wingless and powered lift eVTOL aircraft types for varying mission lengths. For a generic air taxi mission with a payload of 400 kg, the powered lift type demonstrates its mass efficiency when sized for missions above 10 km in range. However, the simpler architecture of the wingless eVTOL aircraft type makes it preferable for missions below 10 km in range when considering energy efficiency. The results of the sizing study were compared against a selection of eVTOL aircraft data. The results showed a good agreement between the estimated aircraft mass using the proposed sizing method and published eVTOL aircraft data.

Keywords: eVTOL sizing; conceptual aircraft design; powered lift; wingless; urban air mobility

Citation: Ugwueze, O.; Statheros, T.; Horri, N.; Bromfield, M.A.; Simo, J. An Efficient and Robust Sizing Method for eVTOL Aircraft Configurations in Conceptual Design. *Aerospace* **2023**, *10*, 311. https://doi.org/10.3390/aerospace10030311

Academic Editor: Bosko Rasuo

Received: 1 October 2022
Revised: 3 March 2023
Accepted: 4 March 2023
Published: 21 March 2023

1. Introduction

The aviation industry is witnessing a disruption in propulsion and energy storage technologies [1,2]. Electric vertical take-off and landing (eVTOL) aircraft appear to be at the forefront of implementing these disruptive technologies [2–4]. By the fourth quarter of 2022, over 500 eVTOL concepts, prototypes, and production vehicles have been unveiled [5]. The European Union Aviation Safety Agency (EASA), through its "Special Condition for Small-Category Vertical Take-Off and Landing Aircraft", has specified that an essential requirement for these aircraft is the vertical take-off and landing capability [6]. These aircraft would also possess fully electric or hybrid-powered propulsion and energy storage systems and be typically designed to carry under ten passengers with a maximum take-off mass below 3175 kg [6]. A significant proportion of these aircraft designs would provide urban air mobility (UAM) solutions [1,7]. There are also numerous designs for personal aerial vehicles (PAV) [8]. Aircraft for both use cases are within the sphere of advanced air mobility (AAM) vehicles. Designing aircraft for these AAM missions could be considered the next frontier in aviation. This belief has been bolstered by improved battery technologies [9], advancements in distributed electric propulsion (DEP) technologies [10], and regulatory receptiveness [6,11].

The infancy of the technologies employed in eVTOL aircraft concepts, the multi-mode capabilities of these aircraft, and the commercial sensitivity in obtaining aircraft performance data make a typical data-driven conceptual design process for these aircraft rather

challenging. Historically, the conceptual design of conventional aircraft followed defined syntheses set out in established texts. Roskam [12–14], Torenbeek [15], Gudmundsson [16], and Raymer [17] provide in-depth literature on the conceptual aircraft design methods for fixed-wing aircraft with accommodations for some experimental aircraft and general home-built aircraft. The literature on conventional rotorcraft design is also widely established, however, somewhat less prevalent than its fixed-wing counterparts.

Nonetheless, Newman [18], Seddon [19], Johnson [20], Prouty [21], and Leishman [22] provide an in-depth look into the governing principles in rotorcraft aerodynamics and performance. In addition, case studies on rotorcraft sizing and, in some cases, the treatments of VTOL aircraft design are covered. The design synthesis covered in the fixed-wing aircraft design literature relies heavily on existing aircraft data from established manufacturers. This approach would be ideal for eVTOL aircraft conceptual design in the future after there is widespread adoption of these aircraft and the availability of comprehensive aircraft performance data from in-service operations. Nevertheless, applying these conventional aircraft mass estimation methods has proven beneficial to the eVTOL aircraft initial sizing. The mass estimates produced from this approach are conservative because most traditional mass estimation models are derived from data on aircraft that employ mostly conventional aerospace alloys in their airframes. eVTOL aircraft, on the other hand, are expected to employ advanced composite materials for most or all of their structural components to keep their empty mass at a minimum.

In line with the rapid development of eVTOL aircraft, research into the conceptual design of eVTOL aircraft has grown recently. There are now several proposed approaches to the conceptual design of fully- and hybrid-electric eVTOL aircraft [23–38]. This is due to the interest in the field, a wide variety of design approaches, and the early-stage development and adoption of these aircraft. Sizing methods, which are methods for estimating an aircraft's mass, layout, geometry, and power requirements to meet mission requirements, have been well-established for conventional fixed-wing aircraft. However, these conventional methods are insufficient for eVTOL aircraft sizing for two main reasons: (1) the distributed electric propulsion systems (DEP) and energy storage technologies used in these aircraft, and (2) the vertical take-off and landing capability of these aircraft [6]. Sizing methods for conventional aircraft are based on liquid fossil fuels, whose mass reduces in flight. Batteries, on the other hand, do not share this trait. Therefore, using batteries as the energy source for eVTOL aircraft is becoming widespread [5]. A sizing method proposed for eVTOL aircraft is expected to account for this peculiarity. As the halfway point between fully-electric and conventional fuel-based aircraft, hybrid-electric aircraft utilise hydrogen fuel cells to generate electric power for the propulsion units [31]. This allows the partial implementation of conventional sizing methods based on fuel fractions due to decreasing aircraft mass during a mission. This is evident in studies focused on the conceptual and preliminary design of hybrid-electric VTOL aircraft [31,35–37,39,40].

Although the literature on the initial sizing of fully-electric or fully-electric eVTOL aircraft has grown recently, it is not as established as that of hybrid-electric aircraft. This may be attributed to the lower range performance of the fully-electric designs compared to their hybrid-electric counterparts. Hybrid-electric aircraft remain the practical option for electric aircraft designed for relatively long-range missions due to the impracticality of fully-electric aircraft designs. However, this has begun to change for aircraft designed for UAM applications at the end of 2021 because of the significant improvements in battery energy densities [41]. The average energy densities for lithium-ion cells were around 250 Wh/kg [9]. Even other battery chemistries, such as lithium–sulphur (Li-S) batteries, show a promising battery density of up to 560 Wh/kg in laboratory conditions [42]. Notable studies on fully-electric eVTOL aircraft sizing include Hepperle [10], Bacchini and Cestino [34,38], and Kadhiresan and Duffy [43]. These studies have developed electric aircraft battery sizing models, eVTOL performance models, and data-driven eVTOL propulsion sizing models. Other studies propose a general sizing methodology that could be applied to fully- and hybrid-electric eVTOL aircraft [23,26,28,43,44].

On the other hand, some sizing studies for eVTOL aircraft have focused on one eVTOL type, wingless [38,44] or powered lift [29,30,45]. In addition, studies focused on the preliminary design stage and optimisation of aircraft parameters [28,43,46] present a comprehensive preliminary design process for fully-electric eVTOL aircraft. However, this preliminary design process may not be the first step for the eVTOL aircraft designer seeking to conduct an initial sizing study using only top-level aircraft requirements, part of the conceptual design process. Finally, some sizing methods have been developed for specific use cases, such as medical emergency services [39], while other studies focus on sizing methodologies for uncrewed aerial vehicles (UAV) [37].

The sizing studies presented so far have significantly improved the body of knowledge in eVTOL aircraft conceptual design. However, as eVTOL aircraft technologies evolve, questions remain about the eVTOL aircraft conceptual design process and its applicability to UAM operations, specifically, the question on improving the robustness and efficiency of the initial sizing methods to allow rapid comparative studies between different eVTOL aircraft types for given mission requirements. These questions are investigated in this paper.

2. eVTOL Aircraft Configurations

It is essential to understand the distinctions between the different types of eVTOL aircraft and how their unique attributes influence the aircraft sizing process. EASA, via its Special Condition for small-category VTOL aircraft (SC-VTOL) [6], has outlined two distinct characteristics common to eVTOL aircraft. These are the vertical take-off and landing (VTOL) capability and a distributed electric propulsion system [6]. The latter allows for less complex applications of propulsion systems for the "vertical lift" and "forward thrust" mode compared to jet engines and their complex thrust vectoring schemes employed by conventional VTOL aircraft. Subsequently, these propulsion units will be referred to as "lift/thrust units" (LTUs), in line with the SC-VTOL nomenclature [6]. EASA also indicates that the VTOL capability of these eVTOL aircraft sufficiently differentiates them from conventional aeroplanes. Likewise, distributed electric propulsion (more than two LTUs) also adequately differentiates eVTOL aircraft from conventional rotorcraft [6,33].

In Figure 1, an illustrated breakdown of eVTOL aircraft types is presented to help the reader visually discern the propulsion configurations of the different eVTOL types. Wingless eVTOL aircraft rely solely on the thrust from their LTUs for both vertical lift and forward flight. Multicopters, as the name suggests, possess multiple LTUs, which can only provide vertical lift, while PAVs are single-seat multicopter eVTOLs where the operator sits or stands to ride the aircraft. All eVTOL aircraft types can take off and land vertically, thus requiring no need for a runway. However, only powered lift aircraft possess wings. This allows them to cruise at similar speeds to conventional fixed-wing aircraft and at significantly higher altitudes than wingless eVTOL aircraft such as multicopters (Figure 2g), hoverbikes (Figure 2h), and electric rotorcraft (Figure 2i). The additional capability of the powered lift aircraft naturally presents opportunities to carry out extended-range missions more efficiently than the wingless type. This allows the aircraft designer the flexibility to exceed the capabilities of the wingless type in terms of cruise speed, payload, and range. This will be explored in the later sections of this paper.

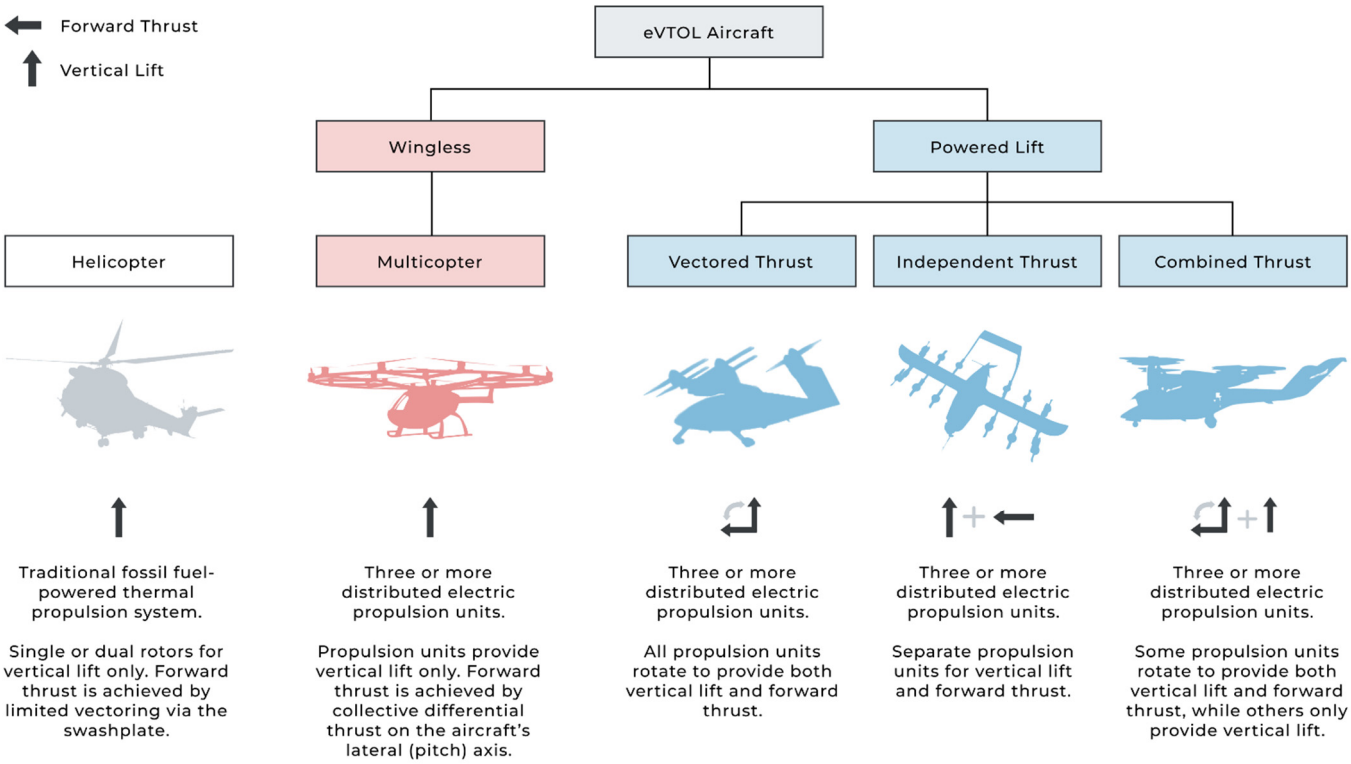

Figure 1. Classification of eVTOL aircraft by their primary propulsion configurations.

However, the powered lift aircraft type's advantages come at a cost. Powered lift aircraft are significantly more complex to design. This is mainly due to two factors:

- The inclusion of a wing and its associated systems for aerodynamic lift during the cruise stage;
- The additional LTUs required for the forward mode and, in some cases, their associated vectoring systems.

The independent thrust eVTOL type entails a separate propulsion for forward thrust during the cruise phase, while the LTUs for vertical lift remain inactive. Likewise, only the LTUs for vertical flight are used during vertical flight, while the forward flight LTUs remain inactive. A reduction in complexity and the overall design cost is another advantage of this eVTOL type. The LTUs in this configuration are considered "deadweight" when inactive, directly contributing to increased drag and overall aircraft mass. eVTOL aircraft designers mitigate the drag issue by locking propellers parallel to the slipstream during the cruise phase. This can be observed in the Eve Air Mobility eVTOL [47] and the Beta Technologies Alia eVTOL (Figure 2e). At the same time, other designs feature stowing the unused vertical lift LTUs in aerodynamic pods or nacelles during cruise [48]. However, even incorporating this feature would add to the overall design complexity.

The vectored thrust types appear to have the most complexity, mainly due to the systems required for vectoring the thrust between the vertical and forward regimes. This problem is not new, as it has been an issue since the development of conventional VTOL aircraft in the 1960s [49]. As a result, many approaches for thrust vectoring that have been developed over time are now being adapted to eVTOL aircraft designs. Tilt-fa and tilt-prop designs rotate only the LTUs, in this case, lift fans (Figure 2b) [50] or propellers (Figure 2a) [51], to activate the vertical lift or forward thrust modes. These are the most common implementation for vectored thrust eVTOL aircraft. Another implementation is the tilt-wing, which rotates the wing and the attached LTUs. The challenge for this type comes in maintaining stability during the transition between the vertical and forward modes [27]. This limitation suggests why fewer concepts are based on this approach, with the Airbus (Acubed) Vahana concept being an example (Figure 2c). A few designs rotate the aircraft's

entire body or structural frame to activate the vertical or forward modes. These are called tilt-body or tail-sitters—a reference to the aircraft's orientation after landing. Examples of this type are the Neoptera eOpter concept [52] and the Opener Blackfly (Figure 2d) [53]. Regardless of vectoring approach, all vectored thrust designs would still require additional systems to control and actuate the vectoring along with appropriate redundancies due to the criticality of these systems, all of which add to the aircraft's empty mass.

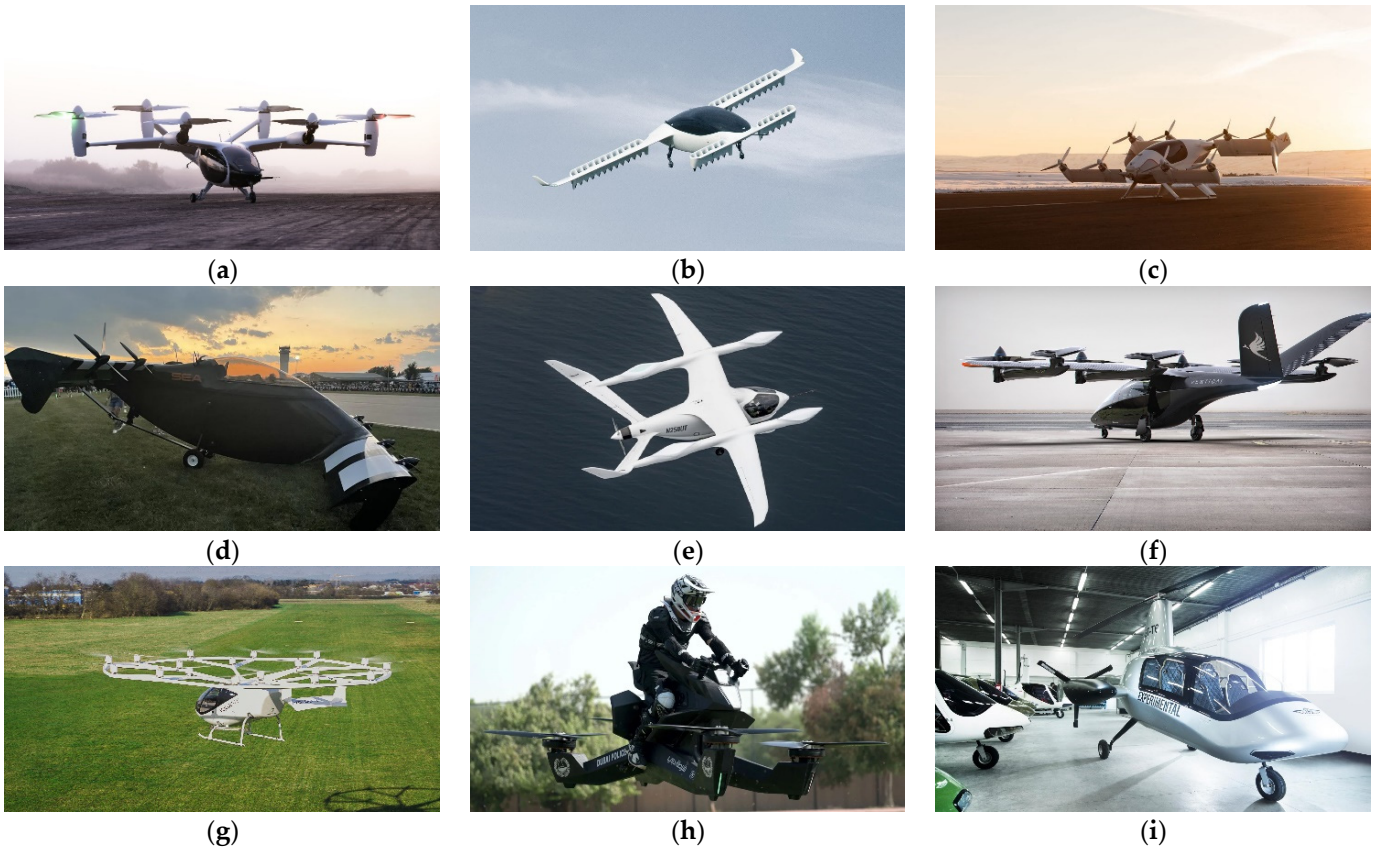

Figure 2. Select eVTOL aircraft with highlighted propulsion configurations: (**a**) Joby Aviation eVTOL [51], Powered Lift, Vectored Thrust (Tilt Prop); (**b**) Lilium Jet [50], Powered Lift, Vectored Thrust (Tilt Fan); (**c**) Airbus (Acubed) Vahana [54], Powered Lift, Vectored Thrust, (Tilt Wing); (**d**) Opener Blackfly [53], Powered Lift, Vectored Thrust, (Tilt Body); (**e**) Beta Technologies Alia [55], Powered Lift, Independent Thrust, (Lift + Cruise); (**f**) Vertical Aerospace VX-4 [56], Powered Lift, Combined Thrust, (Tilt Prop); (**g**) Volocopter VoloCity [57], Wingless, Multicopter; (**h**) Hoversurf Scorpion 3 [58], Wingless, Hoverbike; and (**i**) Aviation Artur Trendak T6 [59], Wingless, Electric Rotorcraft.

Finally, the combined thrust type design incorporates thrust vectoring for some propulsion units while the remaining units are fixed for the vertical mode. The advantage of this type is that it lessens the deadweight problem seen in the independent thrust type because all the propulsion units are used during the vertical mode while the unused propulsion units are "parked" during the forward mode. The number of vectored propulsion units is sized to the power required in the forward mode. Then, additional propulsion units are added to satisfy the power requirements in the vertical mode. However, the combined type still brings its additional mass and complexity. The same complications of the vectored thrust can be seen in this type but to a lower degree—only thrust-vectoring LTUs will contribute to this. On the other hand, the deadweight issue seen in the independent thrust remains minor, as only the additional vertical lift LTUs will contribute to this issue. An example of this design is the Vertical Aerospace VX4 eVTOL aircraft (Figure 2f) [56].

This section has described the added complexity of the powered lift type despite its apparent efficiencies in longer-range missions. It informs the next section, which develops a comprehensive aircraft mass model for both the powered lift and wingless type used in the sizing process.

3. eVTOL Aircraft Mass Modelling

This section focuses on determining the total empty mass of the aircraft for a specified payload. The total mass (m) for an electric aircraft can be described as the sum of its empty mass and the payload mass:

$$m = m_{empty} + m_{payload} \tag{1}$$

The empty mass is composed of the energy system mass (m_b), airframe mass (m_a), and propulsion system mass (m_p):

$$\begin{aligned} m_{empty} &= m_b + m_a + m_p \\ &= m_b + \left(m_w + m_f + m_{t,h} + m_{t,v} + m_{lg}\right) + \left(m_{mot} + m_{prop}\right) \end{aligned} \tag{2}$$

Structures common to both eVTOL aircraft types, powered lift and wingless, include the fuselage (m_f) and landing gear (m_{lg}). Some eVTOL aircraft also use landing skids. However, the landing gear model will be applied to both cases for this study. The wing (m_w), horizontal ($m_{t,h}$), and vertical ($m_{t,v}$) tail structures are included for the powered lift aircraft only. The propulsion system mass is comprised of the motor system (m_{mot}) and propeller (m_{prop}) masses.

Developing an efficient sizing method for eVTOL aircraft requires comprehensive mass estimates of the aircraft's constituent parts. The mass estimation method aims to produce, as accurately as practical, mass breakdowns for a sized aircraft, with sufficient detail for the conceptual design phase. This allows the aircraft designer to quickly identify critical characteristics of the initial aircraft design and further investigate and modify the initial requirements.

3.1. Configuration-Dependent Power Model

Power requirements for a given mission are determined by evaluating the aircraft's physics during each mission phase. For example, the vertical flight mode covers the vertical climb, vertical descent, and hover flight phases (Figure 3).

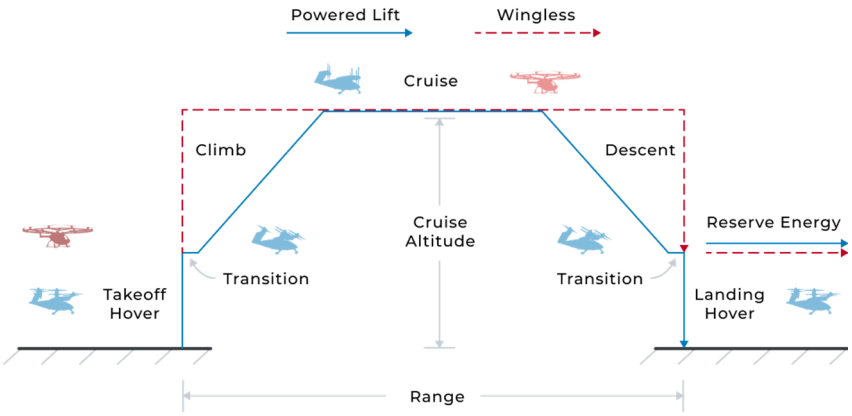

Figure 3. A representative mission profile for the powered lift and wingless eVTOL aircraft types.

During this mode, it is assumed that both the wingless and powered lift eVTOL types are governed by the same physics. Assuming equivalent systems and performance capabilities for the powered lift and wingless eVTOL aircraft, it can be observed that during the vertical mode, the significant difference between the two lies in the presence of a wing on the powered lift eVTOL type. Typical vertical climb rates for helicopters and

VTOL aircraft are around 500 feet per minute or 2.5 m/s [21]. These vertical speeds are significantly low (Mach < 0.01), and because of this, there is a negligible drag effect due to the presence of the wing in the powered lift eVTOL aircraft during the vertical climb or descent. Therefore, in the conceptual design stage, both the powered lift and wingless types can be modelled similarly for hover flight. However, in forward flight (which occurs in the climb, cruise, and descent phases), flight mechanics differ between the two types. Therefore, the powered lift type is treated as a fixed-winged aircraft, and the corresponding fixed-wing power models are applied, albeit with adaptations for a battery energy source. At the same time, the wingless eVTOL type is modelled as rotorcraft in forward flight.

The power required in the vertical mode is modelled with the assumption that the flow through the rotor disk area (A) is one-dimensional, quasi-steady, incompressible, and inviscid [18,22]. This is the actuator disk theory. For a rotorcraft in a hover state, its weight (W) is assumed to be equal to the thrust generated by the rotor disk (T). The ideal power required to hover ($P_{hv,i}$) is obtained from the product of the rotor thrust and the induced velocity (v_i) and given as:

$$P_{hv,i} = Tv_i = \frac{T^{3/2}}{\sqrt{2\rho A}} \tag{3}$$

where ρ is the freestream air density. The term "ideal" indicates that the thrust is generated with an aerodynamic efficiency of 100%. This is true for the assumption of an inviscid flow. However, for realistic estimations of hovering power, a figure of merit (FM) is introduced to account for losses due to the profile drag acting on the rotor blades. The typical values of FM for rotorcraft, applied to eVTOL aircraft, are between 0.5 and 0.8 [22]. The addition of the FM produces the actual power required to hover (P_{hv}). This is given as:

$$P_{hv} = \frac{P_{hv,i}}{\mathrm{FM}} = \frac{T^{3/2}}{\mathrm{FM}\sqrt{2\rho A}} \tag{4}$$

The power required for vertical flight is determined from a ratio of the hover power and the power induced by the relative vertical velocity (V_v) that the aircraft encounters. This is called the power ratio [22]. The power ratio for the climb can be expressed as:

$$\frac{P_{cb}}{P_{hv}} = \frac{V_v}{2\,v_{hv}} + \sqrt{\left(\frac{V_v}{2\,v_{hv}}\right)^2 + 1}, \quad \text{valid for the case } V_v/v_{hv} \geq 0 \tag{5}$$

when the ratio $V_v/v_{hv} \geq 0$, then the aircraft is in the climb phase and $V_{cb} = V_v$. On the other hand, when the ratio $V_v/v_{hv} \leq 0$, then the aircraft is in descent mode and $V_{ds} = V_v$. However, the actuator disk theory struggles to accurately model the descent mode for a range of vertical velocity ratios between $-2 \leq V_v/v_{hv} \leq 0$ [22]. When the vertical velocity ratio falls within this range for a given descent velocity, the hover power equation is used instead of the descent power. This is given as $P_{ds} \approx P_{hv,}$ which is a sufficient approximation for that case. The descent power for the remaining domain of vertical velocity ratios is covered with:

$$\frac{P_{ds}}{P_{hv}} = \frac{V_v}{2\,v_{hv}} + \sqrt{\left(\frac{V_v}{2\,v_{hv}}\right)^2 - 1}, \quad \text{valid for the case } V_v/v_{hv} \leq -2 \tag{6}$$

The implication is that when determining the power required for the descent, the aircraft designer must first calculate the vertical velocity ratio to determine which of the necessary equations to use. The descent power is assumed to be equivalent to the hover power for low descent speeds. However, for higher descent speeds, the descent power is estimated as shown in Equation (6) because the power required to sustain the aircraft at these speeds is now significantly lower than that of hover, is non-negligible, and can be modelled by the actuator disk theory. Equations (4)–(6) complete the power models required for vertical flight.

During cruise, the power required to sustain the wingless eVTOL aircraft type in forward flight ($P_{cr,WL}$) can be expressed as:

$$P_{cr,WL} = T(V_{cr} \sin \alpha + v_i) \tag{7}$$

where V_{cr} is the cruise velocity. The angle of attack (α) is defined as a function of the aircraft's total drag (D) and its thrust (T), where $\alpha = \tan^{-1}(D/T)$ [22,60]. On the other hand, the power required to cruise for the powered lift aircraft type ($P_{cr,PL}$) is given as:

$$P_{cr,PL} = \frac{1}{\eta_{prop}} D\ V_{cr} \tag{8}$$

where η_{prop} is the efficiency of the propulsion system. The total drag for the wingless aircraft includes the parasitic rotor drag and the airframe drag, for both the powered lift and wingless eVTOL aircraft. The drag coefficient of the airframe (c_D) is estimated as:

$$c_D = c_{D_0} + \frac{C_L^2}{\pi \mathrm{AR} e} \tag{9}$$

where the first term on the right-hand side is the zero-lift drag coefficient or parasitic drag (c_{D_0}) and the second term estimates the total induced velocity of all lifting surfaces present. The induced drag is a function of the lift coefficient of the lifting surface (c_L), its aspect ratio (AR), and its Oswald's efficiency factor (e). The drag force on the airframe can then be defined as:

$$D = \frac{1}{2}\rho V_{cr}^2 S c_D = \frac{1}{2}\rho V_{cr}^2 S \left(c_{D_0} + \frac{C_L^2}{\pi \mathrm{AR} e} \right) \tag{10}$$

When determining the cruise power for both eVTOL aircraft types, the drag force experienced by the aircraft largely determines the power required. The induced drag can be estimated both analytically and computationally via CFD analysis. Methods to estimate the parasitic drag are presented in [12,16,17]. For this study, however, NASA's OpenVSP tool was used to estimate the parasitic drag for both aircraft [61,62]. In UAM missions, it is anticipated that eVTOL aircraft will maintain a nominal cruising altitude of approximately 300 m [7]. Since wind speeds typically decrease in an order of magnitude closer to the ground [63], wind interference is assumed to have a minimal effect on aircraft operations at this altitude and cruising speed in the initial sizing study. However, during the preliminary design stage, or when sizing for demanding environments, adjustments may be made to the power requirements and powerplant sizing to ensure that the aircraft's performance and controllability remain within regulated limits [6], even during increased lateral and asymmetric wind conditions where appropriate [64,65].

The power equations for the powered lift and wingless eVTOL aircraft types over the entire mission are summarised in Table 1.

Table 1. Summary of configuration-dependent power models for all mission phases.

Mission Phase		eVTOL Configuration	Power Model
1	Take-off, Hover	Both	$P_{hv} = \frac{T^{3/2}}{\mathrm{FM}\sqrt{2\rho A}}$
2	Climb	Both	$\frac{P_{cb}}{P_{hv}} = \frac{V_v}{2\,v_{hv}} + \sqrt{\left(\frac{V_v}{2\,v_{hv}}\right)^2 + 1}$
3a	Cruise	Powered lift	$P_{cr,PL} = \frac{1}{\eta_{prop}} D\, V_{cr}$
3b	Cruise	Wingless	$P_{cr,WL} = T(V_{cr}\sin\alpha + v_i)$
4	Descent	Both	$\frac{P_{ds}}{P_{hv}} = \frac{V_v}{2\,v_{hv}} + \sqrt{\left(\frac{V_v}{2\,v_{hv}}\right)^2 - 1}$ Only valid for higher descent speeds ($V_{ds}/v_{hv} \leq -2$). For lower descent speeds ($-2 \leq V_{ds}/v_{hv} \leq 0$), the assumption $P_{ds} \approx P_{hv}$ applies.
5	Landing, Hover	Both	The same as Take-off, Hover

3.2. Energy System Mass Model

The energy system has been abstracted to comprise the battery for an initial sizing study in the conceptual aircraft design stage. The mass of the battery energy management systems and thermal protection systems are assumed to include the overall battery mass at this stage. The battery mass is the most significant determinant of the final aircraft mass. The power models presented in the previous section are used to estimate the battery mass. For each mission phase outlined in Table 1, the energy consumed is obtained from the product of the power exerted and the duration of the mission phase. The total energy consumed (E) for the entire mission thus becomes the sum of the energy consumed for n mission phases (j):

$$E = \sum_{j=1}^{n} P_j t_j \tag{11}$$

This energy estimate is also adjusted to account for two aspects. The first is the additional energy required to divert to a suitable airport in an emergency. The distance to the diversion airport (R_{div}) is added to the mission's cruise distance or range requirement. Secondly, the battery's usable capacity is set lower than its total capacity. This is generally at 80% of the total capacity. Thus, the minimum battery state of charge ($\mathrm{SoC_{min}}$) is 20%. Setting the minimum capacity of the battery protects the battery from damage. Multiple charging cycles that completely drain lithium-ion batteries severely affect the longevity of these batteries. Thus, setting a minimum state of charge improves the overall battery life and reduces maintenance costs. Furthermore, a unique situation presents itself for fully-electric eVTOL aircraft operating UAM missions, as these aircraft could also utilise the extra battery reserve if an exceptional emergency occurs at low battery levels, in addition to the initial diversion requirement. Typical lithium-ion battery efficiencies (η_b) are between 80% and 90% [9,66], while typical lithium-ion battery densities (SED) are in the region of 170 Wh/kg to 350 Wh/kg [10,67]. Finally, the battery mass (m_b) can now be calculated from the total energy consumed during the mission and is given as:

$$m_b = \frac{E(1 + \mathrm{SoC_{min}})}{\mathrm{SED}\ \eta_b} \tag{12}$$

3.3. Airframe Mass Model

The airframe component masses from Equation (2) are estimated in this section based on established mass ratios for similar-category aircraft. It is important to note that these mass ratios are obtained from aircraft components made from aerospace-grade aluminium. There is currently no data for mass ratios based on composite materials for comparable aircraft. This is partly due to the commercially sensitive nature of eVTOL aircraft develop-

ment. For this reason, the mass ratios based on aluminium aircraft are used as a stop-gap. However, it will be seen in later sections that for a typical UAM mission, these conservative structural masses do not primarily influence the overall sizing results.

The fuselage is a standard structural component in aircraft. It encloses the occupants, cargo, and often other aircraft systems. Most powered lift and wingless eVTOL concepts have a fuselage. However, there are some wingless PAV aircraft without an enclosure for the occupant; see Figure 2h. Thus, the fuselage model presented below may only be used for applicable aircraft or modified to suit the applicability of the desired study. The fuselage mass model (m_f) is taken from the "Cessna class II method for fuselage mass estimation" implemented in ref [14]. The fuselage length (l_f), maximum fuselage section perimeter (P_{max}), and number of occupants (N_{pax}) are required to use this model. The final fuselage mass is also dependent on the total mass of the aircraft (m). This is true for all the airframe models presented in this section. The fuselage model is valid for general aviation aircraft with an unpressurised fuselage and a maximum cruise speed of 370 kph. The fuselage mass model can be expressed as:

$$m_f = 14.86\, m^{0.144} \left(\frac{l_f}{P_{max}}\right)^{0.778} {l_f}^{0.383}\, {N_{pax}}^{0.455} \tag{13}$$

As the name suggests, the wingless eVTOL aircraft type lacks a wing for aerodynamic flight. Thus, the wing model presented below only applies to the powered lift eVTOL aircraft type. The wing mass model (m_w) is the "Cessna class II method for wing mass estimation" implemented in ref [14]. The wing area (S), design load factor (η_w), and aspect ratio (AR_w) are required to use this model. This model is valid for an aircraft with a cantilever wing and a maximum cruise speed of 370 kph. The wing mass is given as:

$$m_w = 0.04674\, m^{0.397}\, S_w^{0.360}\, {\eta_w}^{0.397}\, \mathrm{AR}_w^{1.712} \tag{14}$$

The empennage consists of the horizontal and vertical tail sections. The empennage mass is modelled using the "Cessna class II method for empennage mass estimation" implemented in ref [14]. As with the wing model, the empennage model depends on the geometric characteristics of the horizontal and vertical tails. For each tail, these are tail area (S_t), tail aspect ratio ($AR_{t,h}$), tail root chord (t_r) and tail quarter chord sweep angle ($\Lambda_{0.25}$). This model is valid for an aircraft with a lightly loaded empennage and no horizontal tail sweep. The horizontal tail ($m_{t,h}$) and vertical tail ($m_{t,v}$) mass models are thus given as:

$$m_{t,h} = \frac{3.184\, m^{0.887}\, {S_{t,h}}^{0.101}\, {\mathrm{AR}_{t,h}}^{0.101}}{174.04\, {t_{r,h}}^{0.223}} \tag{15}$$

$$m_{t,v} = \frac{1.68\, m^{0.567}\, {S_{t,v}}^{1.249}\, {AR_{t,v}}^{0.482}}{639.95\, {t_{r,v}}^{0.747}\, \left(\cos \Lambda_{0.25\ t,v}\right)^{0.882}} \tag{16}$$

The horizontal and vertical tail areas ($S_{t,h}, S_{t,v}$) are estimated by determining the tail volume ratios [16,68]. The thickness-to-chord ratios ($t_{r,h}, t_{r,v}$) are assumed as 10% for both the horizontal and vertical tails.

Finally, the landing gear mass is adapted from the "USAF method for landing gear mass estimation" implemented in ref [14]. An eVTOL aircraft may or may not use a landing gear. Thus, the applicability of the mass model should be evaluated on a case-by-case basis. The landing gear mass model (m_{lg}) depends on the struct length of the landing gear (l_{lg}) and the landing gear design load factor (η_{lg}). This model is valid for a maximum cruise speed of 555 kph. The landing gear mass model is given as:

$$m_{lg} = 0.054\, {l_{lg}}^{0.501} \left(m\, \eta_{lg}\right)^{0.684} \tag{17}$$

3.4. Propulsion System Mass Model

The propulsion system has been abstracted to consist of each electric motor system and its propeller or fan. This is sufficient for an initial sizing study in the conceptual aircraft design stage. Each electric motor system comprises the electric motor, sensors and controller, a cooling system, and an inverter (Figure 4).

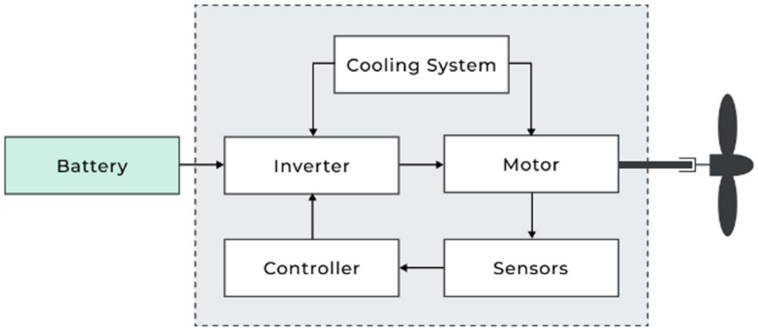

Figure 4. System overview of a typical lift/thrust unit for eVTOL aircraft.

The motors are sized to the maximum power requirement for the entire mission. This is usually in the vertical climb phase. For this method, a power density regression model (Figure 5) is developed from publicly available data on direct current (DC) electric motors used in aerospace applications. The collected motor data is presented in Appendix C.

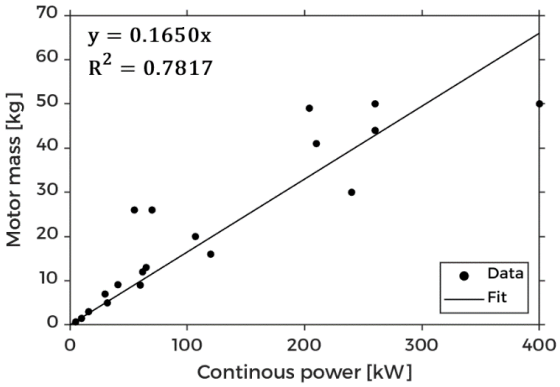

Figure 5. Electric motor power density regression model.

From the regression model in Figure 5 and the climb power (P_{cb}) in Equation (5), a single motor mass (m_{mot}) can be obtained by dividing by the total number of motors or LTUs (N_{mot}). Additionally, a power margin (PM) is included to provide emergency power in the event of a motor failure. This approach is in line with conventional rotorcraft design, and at 50%, it exceeds the typical power margins of conventional helicopters, around 30% [21]. Thus, the motor mass becomes:

$$m_{mot} = 0.165 \frac{P_{cb}\ (1 + \mathrm{PM})}{N_{mot}} \tag{18}$$

If possible, the propeller mass should be obtained directly from manufacturer data. However, in the case where the propeller details are not yet known, which is typical in the initial sizing stage, then the propeller mass (m_{prop}) can be modelled using the "Torenbeek propeller mass estimation method" [14,15]. This model relies on the propeller diameter (d_{prop}), number of blades on the propeller (N_{bl}), and the number of propellers (N_{prop}), which is usually the same as the number of motors (N_{mot}). The model is valid for propellers

intended for motors with a maximum shaft power of 1100 kW. The propeller mass can be expressed as:

$$m_{prop} = 0.144 \left(d_{prop} \frac{P_{cb}}{N_{prop}} N_{bl}^{0.5} \right)^{0.782} \quad (19)$$

In this section, the overall eVTOL aircraft mass model has been presented. This model is made up of three sub-models. These are the battery mass model, the airframe mass model, and the propulsion system model. The battery mass is obtained by analysing the power required over the parts of the entire mission for the related eVTOL aircraft configuration. Once the total power required for the mission is obtained, the energy consumed can be easily estimated. It will be seen later that the battery mass is the primary determinant of the overall aircraft mass, similar to the impact of fuel mass fractions on the final mass of fossil-fuel-powered aircraft, albeit with more importance due to the significantly lower energy densities of current batteries as compared to fossil fuels.

4. Sizing Method

It can be observed from the previous section that the airframe mass models can only estimate a component mass when supplied with the total mass of the aircraft. The implicit problem of a circular dependency becomes evident here as the component mass models rely on a future estimate of the total aircraft mass. This is a fundamental problem in performing aircraft sizing studies. Hence, direct methods cannot be employed to solve this problem. Iterative methods, on the other hand, can be used to obtain a solution. Both open and closed iterative methods can solve this problem. The suitability of the bisection method, which is a closed method, was investigated and confirmed in an earlier study [33]. However, the standard fixed-point iteration, an open method, can also solve the sizing problem and has been employed in multiple eVTOL aircraft sizing studies. Both methods work well but are relatively inefficient when compared to the Newton–Raphson method. The comparative advantage of the NR method is speed. It is significantly faster than the other two methods and is the iterative method of choice for complex root-finding exercises. However, a significant pitfall of the NR method is that it is susceptible to the function's nature and the accuracy of the initial guess [69].

Sizing studies in the conceptual design stage are exploratory. As such, several variables in the mass estimation model shown in the previous section may need to be updated or modified as the search to find a suitable design continues. The standard fixed-point iteration and bisection methods can be used instead of the NR since stability is a priority. However, a concern is that the mass estimation models presented in the previous section and others generally seen in eVTOL sizing studies are bound to become more complex as further research on eVTOL aircraft systems continues. As a result, the computational penalty for running the fixed-point or bisection methods instead of NR or other efficient algorithms would become increasingly non-negligible. Therefore, this section explores hybrid algorithms that combine the stability of fixed-point and bisection methods with the speed of the NR method.

4.1. Bisection

The bisection method, also known as the bracketing method, is a closed method. Therefore, two initial guesses of the aircraft mass are required to begin the incremental search for the root. Furthermore, these values must be selected such that the root lies between the two guesses. The bisection method can be efficiently used when the solution space is large, but the limits are known, for example, sizing an aircraft within the bounds of a regulatory limit such as the maximum mass for the aircraft category. In this case, the bisection method can quickly rule out a bad set of initial design parameters because a solution would conform to the desired bounds. The bisection method iteratively reduces this interval (bracketing) until a solution is found. The root x_0 is defined as $x_0 \in 0$ such that $f(x_0) = 0$. For convergence to occur, f must be real and continuous, and then, for an

interval along f such that a and b are the lower and upper endpoints of the interval. If $f(x_a)f(x_b) < 0$, then a solution lies somewhere in the interval.

4.2. Fixed-Point Iteration

The fixed-point iteration method is also known as the successive substitution or iterative substitution method. It is the simplest of the three methods. It is an open method, requiring one initial guess of the aircraft mass [69]. This makes the method useful for an exploratory sizing process where a reasonable estimate of the upper and lower bounds of the final aircraft mass cannot be made. This method is beneficial for investigating the mass impacts of incorporating new technologies or systems into the overall aircraft. For a function $f(x) = 0$ where $f : \mathbb{R}^k \to \mathbb{R}$ and $x \in S \subset \mathbb{R}^k$, if $f(x_0) = 0$, then x_0 can be solved by characterizing the initial function as $x = g(x)$. The search for the fixed point of g is carried out in the form of $x_{i+1} = g(x_i)$, where x_0 is the fixed point of g. This method has a linear order of convergence.

4.3. Newton–Raphson

The Newton–Raphson (NR) method is a special case of fixed-point iteration. If the initial point is close to the final solution, it rapidly converges to the solution [70]. The NR method minimizes a function f by locally approximating each step by a quadratic function, thus giving the second order of convergence for this method. Similar to the fixed-point equation, the NR method is $x_{i+1} = g(x_i)$, where $g(x_i) = x_i - f(x_i)/f'(x_i)$. The NR method converges when $|g'(x_i)| < 1$ which can be verified with the convergence criteria $|f(x_i)f''(x_i)| < |f'(x_i)|^2$. For this study's implementation of the method, the function derivatives f' and f'' are calculated using the explicit central differences scheme. Finally, the method becomes unstable as $f'(x_i) \to 0$ and fails if $f'(x_i) = 0$.

4.4. Hybrid Methods

The NR method is the fastest of the three methods investigated. However, the NR method can be highly sensitive to the initial guess. A poorly defined starting point could lead to divergence and oscillations, thus making it impossible to converge to a solution. Furthermore, determining the initial guess for the NR method in explorative sizing studies can be challenging. Firstly, depending on the input parameters and individual mass models used, the nature of the overall aircraft mass model may be unknown during the sizing operation. On the other hand, the fixed-point and bisection methods are more accommodating to poorly defined starting points, but they are also significantly slower than the NR method. Secondly, as more research into eVTOL aircraft sizing continues, more complex physics-based models that better describe the mass characteristics of eVTOL aircraft components may be used in the conceptual design stage. This highlights the need for faster and more robust algorithms to carry out the sizing calculations.

Thus, a hybrid of the bisection and NR methods (bisection NR) and a hybrid of the fixed-point and NR methods (fixed-point NR), are studied. These hybrid methods are aimed at current and future more complex mass estimation models. The bisection NR hybrid method begins with the bisection in the first phase until an initial tolerance is reached, the "switch-point tolerance". It then switches to the NR method in the second phase to rapidly converge to the final solution. The fixed-point NR hybrid method only differs from the former by using the fixed-point method in its first phase. The pseudo-codes for both hybrid methods are presented in Algorithms A1 and A2 in Appendix A.

Multiple tests were conducted to assess the correlation between the number of iterations needed to converge and the residual error of mass estimation. This was used to determine the switch-point between the two phases in the hybrid methods. It was observed that within the first five iterations, the bisection and fixed-point methods brought the residual error down to 5% of the final-sized mass. Within this narrowed range, the NR method was guaranteed to converge and performed very well under multiple sizing scenarios for both the powered lift and wingless eVTOL aircraft types.

4.5. Method Evaluation

An initial sizing exercise evaluates the four methods presented in the previous section. Table 2 presents the parameters of a typical UAM mission. The initial sizing exercise compares the sized mass of the powered lift and wingless eVTOL aircraft types.

Table 2. Powered lift and wingless eVTOL aircraft design parameters for the sizing study.

Design Parameter	Value	Applies to
Payload	400 kg	Both
Number of occupants, N_{pax}	4	Both
Figure of merit, FM	0.75	Both
Computed drag coefficient, $c_{D_{PL}}$	0.04353	Powered lift
Computed drag coefficient, $c_{D_{WL}}$	0.04476	Wingless
Propulsion system efficiency, η_{prop}	0.85	Both
Motor, prop count, N_{mot}, N_{prop}	4	Both
Motor power margin, PM	50%	Both
Minimum battery state of charge, SoC_{min}	20%	Both
Battery specific energy density, SED	250 Wh/kg	Both
Battery system efficiency, η_b	0.85	Both
Aerofoil lift coefficient, $c_{L_{PL}}$	1.5	Powered lift
Wing aspect ratio, AR	7.0	Powered lift
Oswald's efficiency factor, e	0.85	Powered lift
Fuselage length, l_f	5.0 m	Both
Fuselage maximum sec tion perimeter, p_{max}	4.71 m	Both

The multicopter was the example configuration for the wingless type, while the vectored thrust was used for the powered lift type. The general aircraft design parameters for the initial sizing study are presented in Table 2. The wingless and powered lift eVTOL aircraft are sized to perform the UAM mission defined in Table 3 with a payload of 400 kg. Using the payload as the initial starting point, all four methods were employed to carry out the sizing for both aircraft.

Table 3. The mission settings for a typical UAM flight. Adapted from Uber [7].

Mission Phase	Duration (min)	Horizontal Speed (km/h)	Distance (km)	Vertical Speed (m/min)	Ending Altitude (m)
Take-off Hover	0.17	0	0	0	1.5
Climb	2	0	0	150	300
Cruise	25	240	100	0	300
Descent	2	0	0	−150	1.5
Landing Hover	0.17	0	0	0	0

From Figure 6, all four methods are observed to converge on the same solution for both the wingless and powered lift aircraft. From the relative compute times in Table 4, the methods that employed bisection were considerably slower than their fixed-point counterparts despite the lower average number of iterations. This is because the bracketing operation is more computationally demanding than the simple iteration process. Due to the wingless type's higher mass, its sizing process took significantly more iteration steps than the powered lift using any method that employed the fixed-point approach. The convergence of all methods validates their use in the eVTOL aircraft sizing process. However, since both hybrid methods show an over 70% improvement in the compute time over their standard counterparts, a preference for their use, where applicable, is justified. The fixed-point NR method is used to perform the next studies.

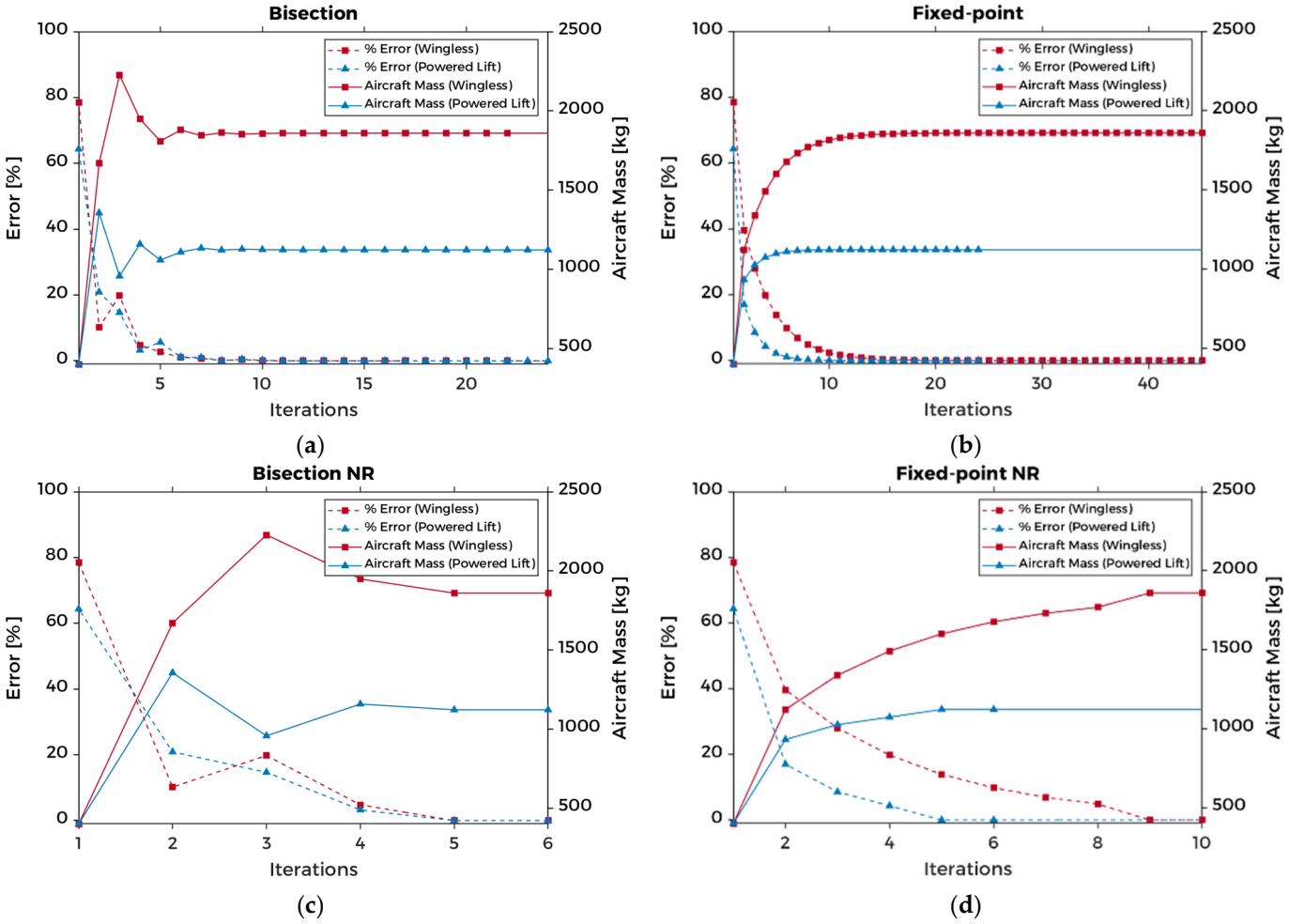

Figure 6. Powered lift and wingless mass estimation and sizing error using (**a**) bisection, (**b**) fixed-point, (**c**) bisection NR hybrid, and (**d**) fixed-point NR hybrid methods.

Table 4. Iterations and compute times using the bisection, fixed-point, and hybrid methods.

Convergence	Bisection	Fixed-Point	Bisection NR	Fixed-Point NR
Average number of iterations	23	35	6	8
Relative compute time	1	0.67	0.27	0.22

5. Sensitivity Analysis

A sensitivity analysis study was carried out to understand the interactions between the many parameters in the design space and how they impact the overall results of the sizing study. The aircraft design parameters and the mission settings outlined in Tables 2 and 3 are used for this study. The disk loading and battery energy density are varied to investigate the sensitivity of other aircraft design parameters to them.

The disk loading is a measure of the aircraft's thrust per disk area DL $= T/A$. It represents the lifting efficiency of a VTOL aircraft, with a low disk loading signifying VTOL aircraft with a higher lifting efficiency and vice versa. VTOL aircraft with a low disk loading typically employ larger rotors or propellers to spread the thrust generated over a larger area, while aircraft with a higher disk loading usually use smaller rotors, propellers, or, most significantly, lift fans. A disk loading range of 400–1000 N/m^2 is used for this analysis and represents typical disk loading metrics for fully-electric eVTOL aircraft [33]. Wing loading is also another metric that is commonly evaluated. However, because this study

compares the powered lift and the wingless eVTOL aircraft types, the usefulness of the wing loading in comparative studies between these two types is little.

Finally, when comparing the relative performance of the wingless and the powered lift eVTOL aircraft types, the battery specific energy density is widely used. The battery mass is the single largest mass constituent of the overall sized aircraft as its mass depends on almost all parameters, such as power estimates, or indirectly, such as the figure of merit. Therefore, evaluating key parameters' effects on the battery mass is necessary. A range of specific energy densities between 250–400 Wh/kg is investigated. The former represents current typical battery technology levels [41], while the latter represents the tipping point for the widescale commercial feasibility of eVTOL aircraft in UAM [2].

5.1. Battery Mass Considerations

Battery mass sensitivity to disk loading and battery energy density for the powered lift and wingless eVTOL aircraft types are presented in Figure 7a,b. Keeping the battery energy density constant, the wingless eVTOL type is significantly more sensitive to disk loading. This is a direct result of its architecture because the wingless eVTOL aircraft relies on its propulsors for vertical lift throughout the mission, unlike the powered lift type, which uses its wing for sustenance during the cruise mode. Therefore, the impact of relying on the vertical lift from the propulsors during hover is significantly less than the wingless eVTOL type. This also suggests why there are significantly more examples of the wingless eVTOL type employing a few large propellers, usually four or eight in a coaxial layout, to improve hover efficiency, as opposed to lift fans with smaller diameters.

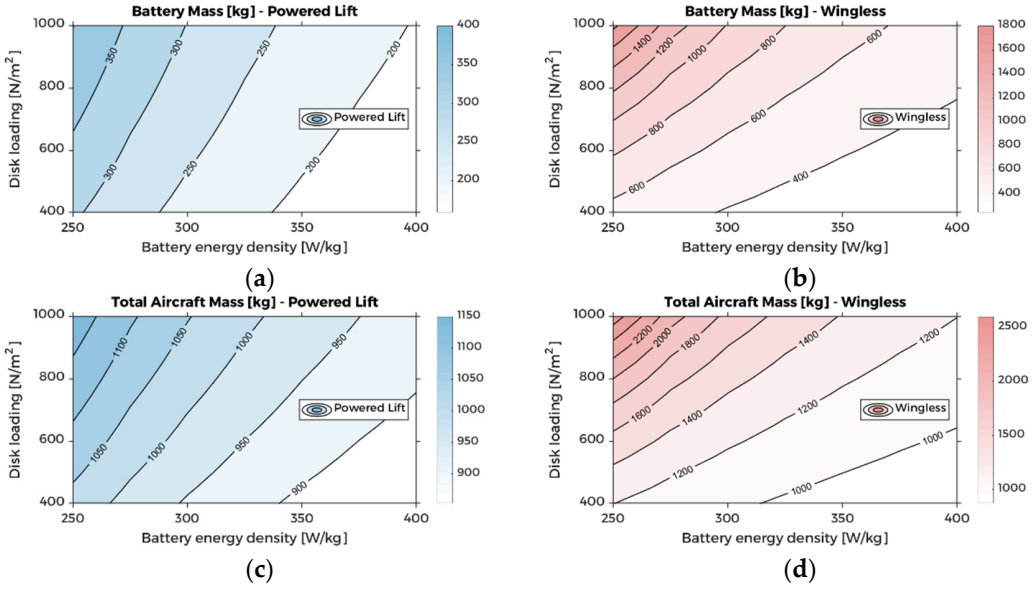

Figure 7. Battery energy density vs. disk loading sensitivity plots for (**a**) powered lift and (**b**) wingless propeller battery mass, and (**c**) powered lift and (**d**) wingless total aircraft mass.

Keeping the disk loading constant, it can be observed that the wingless eVTOL type is also significantly more sensitive to the battery energy density. This again relates to the cruise mode of the aircraft type as more energy is spent in the less efficient cruise mode of the aircraft. Figure 7c,d show the total aircraft mass sensitivity to the same parameters for both the powered lift and wingless eVTOL types. The results largely correlate with the battery mass sensitivity. This outlines the importance of the battery mass to the overall aircraft mass. Even at a high disk loading, an improved battery energy density from 250 to 350 Wh/kg will see the wingless eVTOL type halve its total mass.

5.2. Power and Energy Considerations

A comparison of the power requirements for both the powered lift and wingless eVTOL aircraft types for the hover and cruise modes is shown in Figure 8. The hover power is more sensitive to disk loading for both aircraft types. In contrast, the cruise power is more sensitive to the battery energy density, especially for the powered lift type, due to its lower overall reliance on the vertical lift as a ratio of the total mission power required.

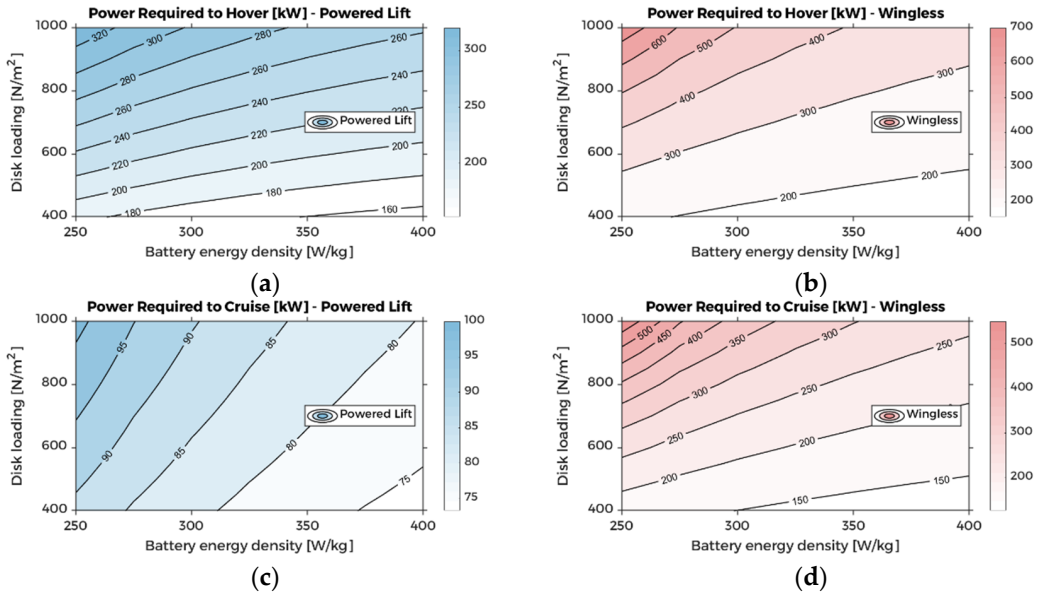

Figure 8. Battery energy density vs. disk loading sensitivity plots for (**a**) powered lift and (**b**) wingless hover power, and (**c**) powered lift and (**d**) wingless cruise power.

A comparison of mission energy consumption for the powered lift and wingless eVTOL aircraft types is presented in Figure 9a,b. These plots give a top-level appreciation of the general efficiency of both aircraft types. The energy efficiency correlates directly with the disk loading and battery density for both aircraft types.

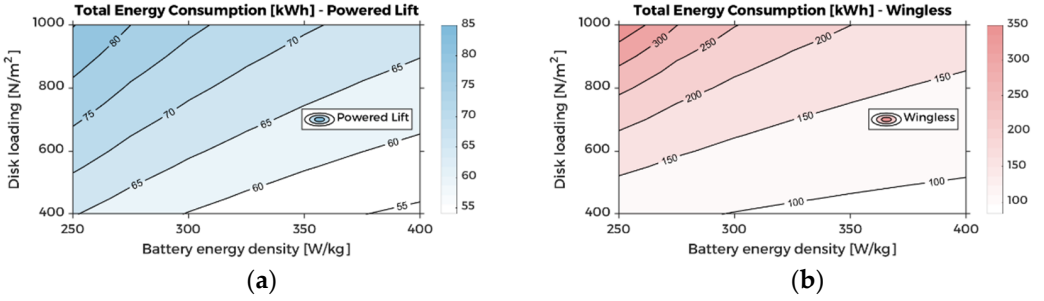

Figure 9. Battery energy density vs. disk loading sensitivity plots for (**a**) powered lift and (**b**) wingless energy consumption.

A common observation among the energy and power requirements presented in Figures 8 and 9 is the significantly higher energy consumption and power requirements for the wingless type due to its reliance on the vertical lift for all phases of flight.

5.3. Wing Considerations

Energy efficiency, the comparative advantage of the powered lift eVTOL aircraft type for UAM missions, has been exemplified in the previous section. The type's overall power and energy requirements are considerably less than the wingless eVTOL aircraft type. This section considers the impacts of the wing design parameters, the aspect ratio, and the

lift coefficient in Figure 10a,b. The aspect ratio of the powered lift aircraft wing affects the overall aircraft mass in two opposing ways. First, the induced lift component of the aircraft drag depends on the wing aspect ratio, shown in Equation (8). A high aspect ratio improves the lifting efficiency of the wing, consequently reducing the drag and aircraft mass. However, Equation (14) shows that increasing the wing's aspect ratio also increases the wing mass because further reinforcement is needed to support the increasingly slender wing, adding more mass in the process. Figure 10a illustrates this situation, and it can be observed that for the specified aircraft and mission settings, the ideal range of aspect ratios for the powered lift type is between 6 and 10. Likewise, in Figure 10b, the impacts of the lift coefficient on the total aircraft mass largely correlate with that of the wing aspect ratio for the same reasons, albeit to a lesser degree.

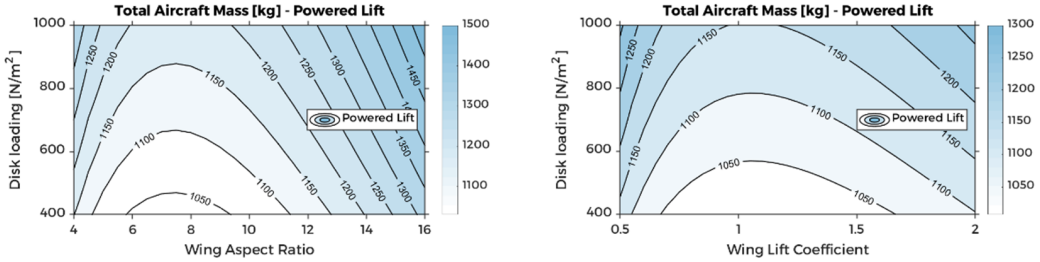

Figure 10. Aircraft mass sensitivities to (**a**) wing aspect ratio and (**b**) wing lift coefficient for the powered lift eVTOL aircraft type.

5.4. Propulsion System Mass Considerations

Figure 11 presents the propeller diameter and propulsion system mass sensitivities to battery energy density and disk loading. The number of propulsion units or LTUs was fixed at four for both the powered lift and wingless eVTOL types. Figure 11a,b show that the propeller diameter is particularly sensitive to disk loading as the propeller diameter effectively determines the disk area when the number of LTUs is fixed. Therefore, the propeller diameter would need to increase by up to 50% or the number of LTUs would need to be increased to achieve lower levels of disk loading and improve hover efficiency.

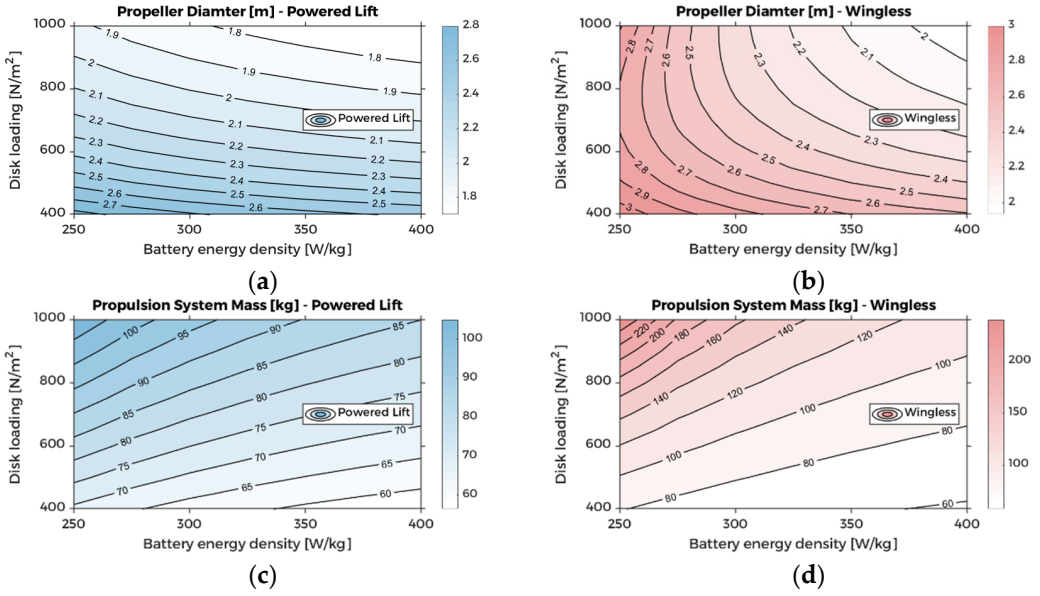

Figure 11. Battery energy density vs. disk loading sensitivity plots for (**a**) powered lift and (**b**) wingless propeller diameter, and (**c**) powered lift and (**d**) wingless propulsion system mass.

In Figure 11c,d, the motor mass dominates the propulsion system mass. This is because the motor mass is sized to the overall aircraft mass. This effect is seen as the propulsion system mass decreases with the decreasing disk loading due to the reduced motor mass, despite an increase in propeller mass as a result of the increasing propeller diameter.

6. UAM Mission Analysis

The sensitivity analysis in the previous section demonstrates the limitations of the wingless eVTOL aircraft type for longer UAM missions where the cruise mode occupies most of the mission time. However, there are questions on the comparative efficiencies for shorter missions. Therefore, in this section, the sizing method developed so far is applied to a comparative study on the mass efficiency of the sized powered lift and wingless eVTOL aircraft.

6.1. Multi-Range Mission Case

Figure 12 shows the results of a multi-range sizing study for the powered lift and wingless eVTOL aircraft types. The study uses the aircraft parameters and the mission settings presented in Tables 2 and 3. However, the battery energy density is increased to 275 kW/kg to represent near-future technology levels. Both aircraft types are sized to carry a payload of 400 kg. The total mass and energy consumption are shown for each eVTOL aircraft type for a given mission range. The sized mass of the wingless type remains below the powered lift type until about the 35 km mission range but then increases above the powered lift type after this point. Furthermore, the energy consumed by the wingless type increases significantly more than the powered lift type as the mission length increases.

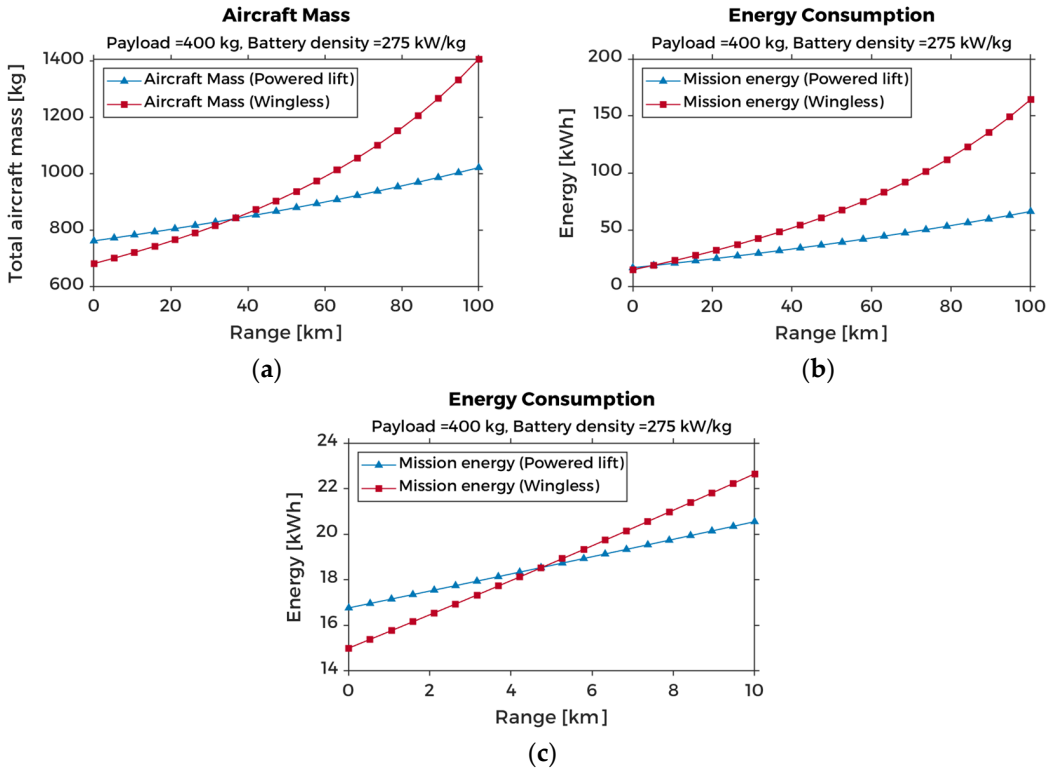

Figure 12. (**a**) Aircraft mass and (**b**,**c**) energy consumption results for powered lift and wingless eVTOL aircraft types up to 100 km range.

However, the results suggest that there is a minimum mission length for which the powered lift type becomes the less favourable option. Figure 12c provides a zoomed-in view of the sub-ten-kilometre mission space. Here, the wingless eVTOL type consumes less energy at missions 5 km or less for this study's aircraft and mission settings. This makes

the wingless type the preferred option for the aircraft designer for very short missions, strictly considering energy efficiency.

Figure 13 compares the mass breakdowns for the powered lift and wingless aircraft at the 37 km range point. Their total masses are equivalent at this point, which is a good point for comparing the mass compositions of both aircraft types. The mass breakdown for both aircraft types shows the payload taking up roughly 47% of both aircraft types, with the remaining 53% as the aircraft's empty mass. The battery mass takes up 24% of the wingless aircraft mass instead of the powered lift type, where the battery mass takes up 16%. This is expected as the wingless aircraft type consumes significantly more energy in the cruise mode. However, the extra structural components needed to allow aerodynamic lift on the powered lift take up 28% of its total mass, contrasting with the wingless type at 20%.

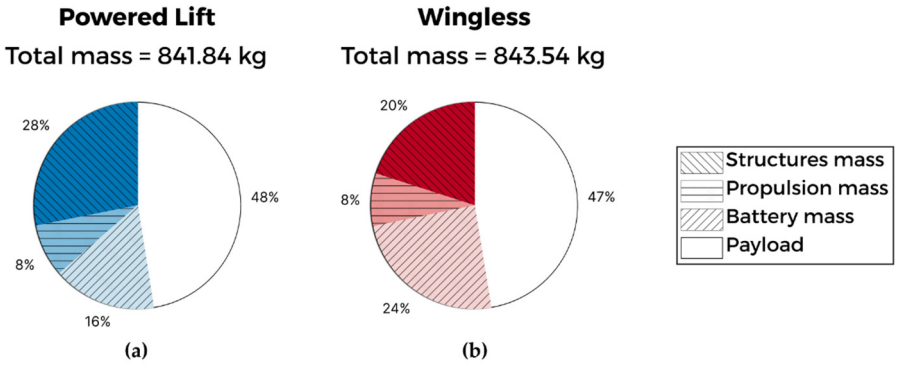

Figure 13. Aircraft mass breakdown for (**a**) powered lift and (**b**) wingless eVTOL aircraft types.

Table 5 provides a clearer picture of the airframe mass breakdown for both types. The powered lift type has effectively traded increased structural mass for gains in battery mass savings, compared with the wingless type at roughly the same mass and range capability. The opposite is true for the wingless type. Finally, the propulsion system remains constant across both types, as this scales with the overall aircraft mass, irrespective of the airframe mass.

Table 5. Airframe component mass breakdown for powered lift and wingless eVTOL aircraft types.

Airframe Component Masses	Powered Lift (kg)	Wingless (kg)	Δ (%)
Fuselage	156.97	157.01	0.03
Wing	54.99	-	-
Horizontal stabiliser	11.8	-	-
Vertical stabiliser	1.22	-	-
Landing gear	11.90	11.92	0.14
Total airframe mass	236.88	168.93	28.69

6.2. Comparison with eVTOL Aircraft Data

A pre-validation of the sizing method developed so far is presented in this section. The results of the powered lift and wingless eVTOL aircraft multi-range sizing study were compared with the eVTOL aircraft data made publicly available by some eVTOL developers. Appendix B shows the eVTOL aircraft data used in this study. Using the same UAM mission settings and aircraft parameters from the previous case study, the powered lift and wingless eVTOL aircraft are sized for a series of aircraft ranges. For the powered lift aircraft, this is between 1 and 330 km. For the wingless aircraft type, it is between 1 and 100 km. eVTOL aircraft mass, payload, and range data were obtained from the manufacturers' websites. Only fully-electric eVTOL aircraft, at least in the sub-scale prototype development stage, were considered. More powered lift eVTOL aircraft with 400–500 kg payloads were found online. Therefore, the study used this payload range to allow a sizeable sample size. These aircraft also typically have between four to five

occupants. For the wingless type, the payload range was between 75–150 kg, with occupant capacities around 1 or 2.

Figure 14a shows the sizing results of the powered lift eVTOL aircraft type. An average payload of 450 kg was used to carry out the sizing. Figure 14b shows sizing results for the wingless eVTOL aircraft type. An average payload of 100 kg was used for this type. Battery energy densities for eVTOL aircraft are rarely made publicly available. Therefore, a 275 kW/kg battery energy density was selected based on independent analyses and current battery energy density projections. Both figures show a general trend between the estimated aircraft mass using the proposed sizing method and eVTOL aircraft data published online by the developers. The observable scatter could be due to several factors, some of which have been identified and explained below.

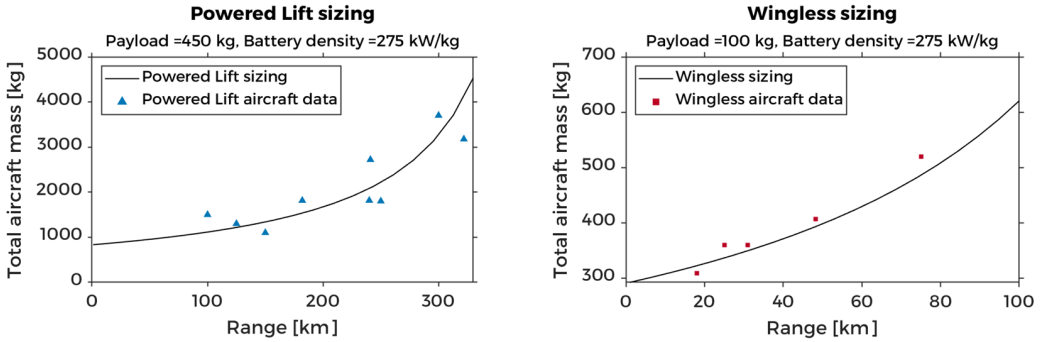

Figure 14. (**a**) Powered lift sizing result compared with powered lift eVTOL aircraft data and (**b**) wingless sizing result compared with wingless eVTOL aircraft data.

Firstly, the sizing results are based on an average payload. For example, the range of payloads for the powered lift aircraft obtained was between 400–500 kg. Therefore, a reason for the scatter is attributed to the selected aircraft's varying payloads. Secondly, the sizing results are generalised for the powered lift and wingless types. However, the aircraft data for the powered lift type consists of some vectored thrust and independent thrust configurations. Thus, part of the scatter can also be attributed to this reason. Thirdly, some scatter could also be attributed to differences in the aircraft structural makeup. For example, different composite structures or lightweight technologies will likely be employed in the aircraft assessed, which is not accounted for in the sizing method.

Finally, the aircraft data used in this study were obtained from information published by the respective eVTOL developers. However, these aircraft parameters are not fully verified since the eVTOL concepts have not yet been fully certified or begun in-service operations. Although steps were taken to ensure a degree of integrity, such as only using data from aircraft concepts that have at least demonstrated prototype flights, there remains a likelihood that some of the stated aircraft parameters may be updated as the eVTOL concepts progress towards certification and in-service operations. For these reasons, the results presented in this section may only serve to validate the sizing method for the wingless and powered lift eVTOL aircraft types in the conceptual design stage within the mission ranges and payloads that have been investigated.

7. Conclusions

A sizing method to rapidly estimate key eVTOL aircraft parameters in the conceptual aircraft design stage has been presented in this paper. This method is employed to conduct comparative studies on the two main eVTOL aircraft classes, the powered lift and wingless types. First, the aircraft mass modelling section defined the overall eVTOL aircraft mass model. This model comprises three parts. These are the battery mass model, the airframe mass model and the propulsion system model. The battery mass is obtained by analysing the power required over the parts of the entire mission for the related eVTOL aircraft

configuration. Once the total power required for the mission is obtained, the energy consumed can be easily estimated. The battery is then sized to deliver the resulting energy estimate. This energy estimate is also adjusted to account for two factors. These are (1) the additional energy required for a diversion to a suitable airport in an emergency and (2) a maximum utilisation of 80% of its state of charge to improve the battery's longevity.

The bisection and fixed-point numerical methods were applied to solve the sizing problem. Both methods solve the problem but are significantly less efficient than the NR method in terms of the number of iterations to reach an accurate solution. However, the NR method is not reliable to use on its own because it can become unstable if a poor initial guess is provided or the sizing equation is modified. Therefore, two hybrid methods are employed to maintain the robustness of the bisection or fixed-point methods and the efficiency of the NR method. These are a hybrid of the bisection and NR methods—Bisection NR and a hybrid of the fixed-point and NR methods—Fixed-point NR. These hybrid methods begin with the bisection or the fixed-point phase and then switch to the NR phase when the range of possible solutions has been narrowed down to within 5% of the solution. The convergence of the standard and hybrid methods validates their use in the eVTOL aircraft sizing process. However, the improved convergence efficiency of the hybrid methods, which is at least 70% faster than the standard methods, and their applicability to more complex sizing problems justify their use. The Fixed-point NR hybrid method is the faster of the two, and it can be used for exploratory sizing studies that are not bound to a range of feasible solutions. On the other hand, the Bisection NR hybrid method can quickly rule out solutions that do not lie within the defined bounds for a feasible solution.

From the sensitivity analysis of the powered lift configuration, increasing the lifting efficiency of the wing was found to improve the aircraft's energy efficiency, but this leads to an increased wing mass and structural support mass. The sensitivity analysis of battery energy density and disk loading for both eVTOL aircraft types reveals the higher energy consumption and power requirements of the wingless eVTOL aircraft type due to its reliance on vertical lift for all phases of flight.

The sizing method compared the powered lift and wingless eVTOL aircraft configurations for multi-range UAM missions with a 400 kg payload. As expected, the powered lift type is more energy efficient for medium to long-range UAM missions. However, the question on the comparative efficiencies of both types at shorter missions are investigated. The powered lift type is more mass-efficient when sized for missions above 10 km, while the wingless type becomes more mass-efficient for missions below 10 km. The results of the sizing study were compared against existing eVTOL aircraft performance data and showed a general trend between the estimated aircraft mass using the sizing method and published eVTOL aircraft data. The results of this study are promising and indicate that the proposed sizing method is potentially valid for the powered lift and wingless eVTOL configurations carrying out UAM missions specified in the study.

The comparative mass efficiencies of the powered lift and wingless eVTOL aircraft types have been investigated in this paper. Therefore, the next step would be to assess the comparative mass efficiencies of the subclasses of the powered lift and wingless eVTOL aircraft types. The robust sizing method presented in this paper could be used to quickly assess the suitability of the main eVTOL configurations, the powered lift and wingless types, for a given mission role in the conceptual design stage. Furthermore, the opportunity is identified to extend the method onto the powered lift and wingless eVTOL aircraft subclasses.

Author Contributions: Conceptualization, O.U., T.S. and N.H.; Methodology, O.U., T.S. and N.H.; Software, O.U.; Data curation, O.U.; Results analysis and validation, O.U., N.H., T.S., J.S. and M.A.B.; Writing—Original draft, O.U.; Writing—Review, editing and approval, T.S., M.A.B., J.S., N.H. and O.U.; Supervision and project administration, T.S. and J.S. All authors have read and agreed to the published version of the manuscript.

Funding: This research received no external funding.

Data Availability Statement: All data are contained within the article.

Conflicts of Interest: The authors declare no conflict of interest.

Nomenclature

A	area [m^2]
AR	aspect ratio
D	drag [N]
DL	disk loading [N/m^2]
E	energy (electric) [kWh]
FM	figure of merit
L	lift [N]
N	number, count
P	power [W]
p_{max}	fuselage maximum section perimeter [m]
PM	power margin
R	range (distance) [km]
S	surface area [m^2]
SED	specific energy density [Wh/kg]
SoC	(battery) state of charge
T	thrust [N]
V	velocity [m/s]
W	weight [N]
$\Lambda_{0.25}$	quarter chord sweep angle [deg]
c_D	drag coefficient
c_L	lift coefficient
d	diameter [m]
e	Oswald's efficiency factor
l	length [m]
m	mass, total mass [kg]
α	angle of attack [deg]
η	efficiency, design load factor
ρ	(air) density [kg/m^3]
R_{res}	reserve diversion range [km]
t_r	maximum tail root thickness [m]
Subscripts	
h	horizontal
hv	hover
b	battery
bl	(rotor or propeller) blade
cb	climb
cr	cruise
ds	descent
f	fuselage
lg	landing gear
max	maximum
min	minimum
mot	motor
$prop$	propeller
t	tail
ult	ultimate
v	vertical
w	wing

Acronyms

AAM	Advanced Air Mobility
DEP	Distributed Electric Propulsion
EASA	European Union Aviation Safety Agency
EPU	Electric Propulsion Unit
ESC	Electronic Speed Controller
eVTOL	electric Vertical Take-Off and Landing
LTU	Lift/Thrust Unit
NR	Newton–Raphson (method)
PAV	Personal Aerial Vehicle
PL	Powered Lift (eVTOL aircraft)
UAM	Urban Air Mobility
UAV	Uncrewed Aerial Vehicle
WL	Wingless (eVTOL aircraft)

Appendix A

The algorithm flow for the Bisection NR and Fixed-point NR methods are shown in Algorithms A1 and A2.

Algorithm A1 Bisection NR algorithm flow

Inputs:
  $\boldsymbol{x_a}$: Initial guess mass, lower bound, and $x_a = m_{payload}$
  $\boldsymbol{x_b}$: Initial guess mass, upper bound. Must satisfy $f(x_a)f(x_b) < 0$
  $\boldsymbol{e_1}$: Switch-point tolerance
  $\boldsymbol{e_2}$: Final tolerance
  $\boldsymbol{n}$**:** Maximum iterations
$x_c = \frac{x_a + x_b}{2}$ (Bisection calculation)
$i = 1$ (Initialize iteration)
while $i < n$
  if $f(x_a) \cdot f(x_b) < 0$ **then**
    $x_b = x_c$
  else
    $x_a = x_c$
end if
  if $|f(x_c)| = 0$ (Exact solution found using bisection)
    return x_c, i
  else if $|f(x_c)| < e_1$ (Switch condition)
    while $i < n$ (Begin NR subroutine)
      $i = i + 1$ (Increase subroutine step)
      $x_i = x_c$
      $x_{i+1} = x_i - \frac{f(x_i)}{f'(x_i)}$ (NR calculation)
      if $|x_i - x_{i-1}| = 0$ **or** $|x_i - x_{i-1}| < e_2$ (Solution found using NR)
        return x_i, i
    end if
    end while
  end if
  $i = i + 1$ (Increase step)
end while

Algorithm A2 Fixed-point NR algorithm flow

Inputs:
x_0: Initial guess mass and $x_0 = m_{payload}$
e_1: Switch-point tolerance
e_2: Final tolerance
n: Maximum iterations
Define $f(x)$ and $g(x)$ such that $x = g(x)$ and $|g'(x) < 1|$
$i = 1$, $x_1 = x_0$ (Initialize iteration)
while $i < n$
  $i = i + 1$ (Increase step)
  $x_i = g(x_{i-1})$ (Fixed-point calculation)
  if $|x_i - x_{i-1}| = 0$ (Exact solution found using fixed-point)
    return x_i , i
  else if $|x_i - x_{i-1}| < e_1$ (Switch condition)
    while $i < n$ (Begin NR subroutine)
      $i = i + 1$ (Increase subroutine step)
      $x_{i+1} = x_i - \frac{f(x_i)}{f'(x_i)}$ (NR calculation)
      if $|x_i - x_{i-1}| = 0$ **or** $|x_i - x_{i-1}| < e_2$ (Solution found using NR)
        return x_i, i
      end if
    end while
  end if
end while

Appendix B

Table A1 presents a list of fully-electric versions of eVTOL aircraft with their performance data used to carry out the pre-validation study. The information presented is sourced from the publicly available data on eVTOL range, payload, and mass.

Table A1. Select eVTOL aircraft performance data.

Name	Developer	Country Code (ISO2 [71])	Primary Class	Range (km)	Payload (kg)	Mass (kg)	Source
Acubed Vahana	Airbus	US	PL	96.6	204.1	930.0	[54]
AMVA	Micor Technologies	US	PL	125.0	450.0	1300.0	[72]
EHang 184	EHang	CN	WL	31.0	100.0	360.0	[73]
Elroy	Astro Aerospace	US	WL	25.0	120.0	360.0	[74]
Esinti	Turkish Technic	TR	WL	48.3	79.8	406.9	[75]
Flyer	Kitty Hawk	US	WL	10.7	99.8	213.2	[76]
Flyka eVTOL	Flyka	RU	WL	75.0	130.0	520.0	[77]
HEXA	LIFT Aircraft	US	WL	18.1	113.4	309.3	[78]
Joby eVTOL	Joby Aviation	US	PL	160.9	90.7	226.8	[51]
Lilium (5-seater)	Lilium	DE	PL	250	*500*	1800	[5]
LimoConnect	Limosa	CA	PL	321.9	499.0	3175.1	[79]
Volocopter (2-seater)	Volocopter	DE	WL	27.4	158.8	449.1	[57]
Voyager X2	XPeng	CN	WL	76.0	200.0	560.2	[80]
VTOL	Napoleon Aero	RU	PL	100.0	400.0	1500.0	[81]

Appendix C

The power density regression model shown in Figure 5 was developed using the electric motor mass and power data below.

Table A2. Electric motor performance data.

Motor(s)	Power (kW)	Mass (kg)	Source
Emrax 188	52	7	[82]
Emrax 208	68	9.1	[82]
Emrax 228	109	12	[82]
Emrax 268	200	20	[82]
Emrax 348	380	41	[82]
MAGicALL MAGiDRIVE 12	12	1.5	[83]
MAGicALL MAGiDRIVE 150	150	16	[83]
MAGicALL MAGiDRIVE 20	20	3	[83]
MAGicALL MAGiDRIVE 300	300	30	[83]
MAGicALL MAGiDRIVE 40	40	5	[83]
MAGicALL MAGiDRIVE 500	500	50	[83]
MAGicALL MAGiDRIVE 6	6	0.7	[83]
MAGicALL MAGiDRIVE 75	75	9	[83]
Magnix magni350 EPU	350	111.5	[84]
Magnix magni650 EPU	640	200	[84]
Siemens SP200D	204	49	[85]
Siemens SP260D	260	50	[85]
Siemens SP260D-A	260	44	[85]
Siemens SP55D	72	26	[85]
Siemens SP70D	92	26	[85]
Siemens SP90G	65	13	[85]
Yuneec Power Drive 10	10	4.5	[86]
Yuneec Power Drive 20	20	8.2	[86]
Yuneec Power Drive 40	40	19	[86]
Yuneec Power Drive 60	60	30	[86]

References

1. Bromfield, M.A. Urban Air Mobility—Human Factors Considerations. In Proceedings of the Chartered Institute of Ergonomics & Human Factors—Human Factors in Future Transportation Conference, Birmingham, UK, 18–19 June 2018.
2. Uber Elevate. Fast-Forwarding to the Future of On-Demand, Urban Air Transportation. Available online: https://www.uber.com/elevate.pdf (accessed on 22 June 2018).
3. Datta, A. *Commercial Intra-City On-Demand Electric-VTOL Status of Technology*; AHS/NARI Transformative Vertical Flight Working Group-2, San Fransisco, CA, USA, 15 January 2018. Available online: https://vtol.org/files/dmfile/TVF.WG2.YR2017draft.pdf (accessed on 1 August 2018).
4. Doo, J.T.; Pavel, M.D.; Didey, A.; Hange, C.; Diller, N.P.; Tsairides, M.A.; Smith, M.; Bennet, E.; Bromfield, M.; Mooberry, J. *NASA Electric Vertical Takeoff and Landing (eVTOL) Aircraft Technology for Public Services—A White Paper*; 20205000636; National Aeronautics and Space Administration: Washington, DC, USA, 1 August 2021. Available online: https://ntrs.nasa.gov/citations/20205000636 (accessed on 24 September 2022).
5. Vertical Flight Society. The Electric VTOL News—eVTOL Aircraft Directory. Available online: http://evtol.news/aircraft (accessed on 12 December 2022).
6. EASA. *Special Condition for Small-Category Vertical Take-Off and Landing (VTOL) Aircraft*; European Aviation Safety Agency: Brussels, Belgium, 2019; Volume SC-VTOL-01.
7. Uber Elevate. Uber Elevate Mission and Vehicle Requirements. Available online: https://s3.amazonaws.com/uber-static/elevate/Summary+Mission+and+Requirements.pdf (accessed on 1 August 2018).
8. Liu, Y.; Kreimeier, M.; Stumpf, E.; Zhou, Y.; Liu, H. Overview of recent endeavors on personal aerial vehicles: A focus on the US and Europe led research activities. *Prog. Aerosp. Sci.* **2017**, *91*, 53–66. [CrossRef]
9. Yu, X.; Sandhu, N.S.; Yang, Z.; Zheng, M. Suitability of energy sources for automotive application—A review. *Appl. Energy* **2020**, *271*, 115169. [CrossRef]
10. Hepperle, M. *Electric Flight—Potential and Limitations; STO-MP-AVT-209*; Institute of Aerodynamics and Flow Technology Braunschweig: Brunswick, Germany, 2012. Available online: https://elib.dlr.de/78726/1/MP-AVT-209-09.pdf (accessed on 1 August 2018).
11. FAA; CAA. Joint FAA and United Kingdom CAA Statement on eVTOL Aircraft. Available online: https://www.faa.gov/newsroom/joint-faa-and-united-kingdom-caa-statement-evtol-aircraft (accessed on 20 May 2022).
12. Roskam, J. *Airplane Design—Part I: Preliminary Sizing of Airplanes*; Design, Analysis and Research Corporation (DARCorporation): Lawrence, Kansas, 2018.
13. Roskam, J. *Airplane Design—Part II: Preliminary Configuration Design and Integration of the Propulsion System*; Design, Analysis and Research Corporation (DARCorporation): Lawrence, Kansas, 2018.

14. Roskam, J. *Airplane Design—Part V: Component Weight Estimation*; Design, Analysis and Research Corporation (DARCorporation): Lawrence, Kansas, 2018.
15. Torenbeek, E. *Synthesis of Subsonic Airplane Design*, 1st ed.; Springer: Dordrecht, The Netherlands, 1982. [CrossRef]
16. Gudmundsson, S. *General Aviation Aircraft Design: Applied Methods and Procedures*; Elsevier Inc.: Oxford, UK, 2014.
17. Raymer, D.P. *Aircraft Design: A Conceptual Approach*, 4th ed.; American Institute of Aeronautics and Astronautics, Inc.: Reston, Virginia, 2006.
18. Newman, S. *The foundations of Helicopter Flight*; Butterworth Heinemann: Oxford, UK; Burlington, MA, Canada, 2003.
19. Newman, J.S.S. *Basic Helicopter Aerodynamics*, 3rd ed.; John Wiley & Sons, Ltd.: Chichester, UK, 2011. [CrossRef]
20. Johnson, W. *Helicopter Theory*; Dover Publications, Inc.: New York, NY, USA, 1980.
21. Prouty, R.W. *Helicopter Performance, Stability, and Control*; Robert, E., Ed.; Krieger Publishing Company: Malabar, FL, USA, 1990.
22. Leishman, J.G. *Principles of Helicopter Aerodynamics*, 2nd ed.; Cambridge University Press: New York, NY, USA, 2006.
23. Palaia, G.; Zanetti, D.; Abu Salem, K.; Cipolla, V.; Binante, V. THEA-CODE: A design tool for the conceptual design of hybrid-electric aircraft with conventional or unconventional airframe configurations. *Mech. Ind.* **2021**, *22*, 19. [CrossRef]
24. Bacchini, A.; Cestino, E.; Van Magill, B.; Verstraete, D. Impact of lift propeller drag on the performance of eVTOL lift+cruise aircraft. *Aerosp. Sci. Technol.* **2021**, *109*, 106429. [CrossRef]
25. Brown, A.; Harris, W.L. Vehicle Design and Optimization Model for Urban Air Mobility. *J. Aircr.* **2020**, *57*, 1003–1013. [CrossRef]
26. Palaia, G.; Abu Salem, K.; Cipolla, V.; Binante, V.; Zanetti, D. A Conceptual Design Methodology for e-VTOL Aircraft for Urban Air Mobility. *Appl. Sci.* **2021**, *11*, 10815. [CrossRef]
27. Chauhan, S.S.; Martins, J.R.R.A. Tilt-Wing eVTOL Takeoff Trajectory Optimization. *J. Aircr.* **2020**, *57*, 93–112. [CrossRef]
28. Riboldi, C.E.D.; Gualdoni, F.; Trainelli, L. Preliminary weight sizing of light pure-electric and hybrid-electric aircraft. *Transp. Res. Procedia* **2018**, *29*, 376–389. [CrossRef]
29. Tyan, M.; Nguyen, N.V.; Kim, S.; Lee, J.-W. Comprehensive preliminary sizing/resizing method for a fixed wing—VTOL electric UAV. *Aerosp. Sci. Technol.* **2017**, *71*, 30–41. [CrossRef]
30. Lee, B.-S.; Tullu, A.; Hwang, H.-Y. Optimal Design and Design Parameter Sensitivity Analyses of an eVTOL PAV in the Conceptual Design Phase. *Appl. Sci.* **2020**, *10*, 5112. [CrossRef]
31. An, J.-H.; Kwon, D.-Y.; Jeon, K.-S.; Tyan, M.; Lee, J.-W. Advanced Sizing Methodology for a Multi-Mode eVTOL UAV Powered by a Hydrogen Fuel Cell and Battery. *Aerospace* **2022**, *9*, 71. [CrossRef]
32. Govindarajan, B.; Sridharan, A. Conceptual Sizing of Vertical Lift Package Delivery Platforms. *J. Aircr.* **2020**, *57*, 1170–1188. [CrossRef]
33. Ugwueze, O.; Statheros, T.; Horri, N.; Innocente, M.; Bromfield, M. Investigation of a Mission-based Sizing Method for Electric VTOL Aircraft Preliminary Design. In Proceedings of the AIAA SCITECH 2022 Forum, San Diego, CA, USA, 3–7 January 2022. [CrossRef]
34. Bacchini, A.; Cestino, E. Electric VTOL Configurations Comparison. *Aerospace* **2019**, *6*, 26. [CrossRef]
35. Vries, R.d.; Brown, M.T.; Vos, R. A Preliminary Sizing Method for Hybrid-Electric Aircraft Including Aero-Propulsive Interaction Effects. In Proceedings of the Aviation Technology, Integration, and Operations Conference, Atlanta, Georgia, 25–29 June 2018. [CrossRef]
36. Finger, D.F.; Bil, C.; Braun, C. Initial Sizing Methodology for Hybrid-Electric General Aviation Aircraft. *J. Aircr.* **2020**, *57*, 245–255. [CrossRef]
37. Kamal, A.M.; Alex, R.-S. Design methodology for hybrid (VTOL + Fixed Wing) unmanned aerial vehicles. *Aeron. Aero. Open Access J.* **2018**, *2*, 165–176. [CrossRef]
38. Bacchini, A.; Cestino, E. Key aspects of electric vertical take-off and landing conceptual design. *Proc. Inst. Mech. Eng. Part G J. Aerosp. Eng.* **2020**, *234*, 774–787. [CrossRef]
39. Barra, F.; Capone, P.; Guglieri, G. A Methodology for Preliminary Performance Estimation of a Hybrid-Electric Tilt-Wing Aircraft for Emergency Medical Services. In Proceedings of the 2020 International Conference on Unmanned Aircraft Systems (ICUAS), Athens, Greece, 1–4 September 2020; pp. 1636–1643. [CrossRef]
40. Cakin, U.; Kaçan, Z.; Aydogan, Z.A.; Kuvvetli, I. Initial Sizing of Hybrid Electric VTOL Aircraft for Intercity Urban Air Mobility. In Proceedings of the AIAA Aviation 2020 Forum, Virtual Event, 15–19 June 2020. [CrossRef]
41. Sripad, S.; Viswanathan, V. The promise of energy-efficient battery-powered urban aircraft. *Proc. Natl. Acad. Sci. USA* **2021**, *118*, e2111164118. [CrossRef]
42. Yin, F.; Jin, Q.; Gao, H.; Zhang, X.; Zhang, Z. A strategy to achieve high loading and high energy density Li-S batteries. *J. Energy Chem.* **2021**, *53*, 340–346. [CrossRef]
43. Kadhiresan, A.R.; Duffy, M.J. Conceptual Design and Mission Analysis for eVTOL Urban Air Mobility Flight Vehicle Configurations. In *AIAA Aviation 2019 Forum*; American Institute of Aeronautics and Astronautics: Dallas, TX, USA, 2019. [CrossRef]
44. Hascaryo, R.W.; Merret, J.M. Configuration-Independent Initial Sizing Method for UAM/eVTOL Vehicles. In *AIAA AVIATION FORUM*; American Institute of Aeronautics and Astronautics: Dallas, TX, USA, 2020. [CrossRef]
45. Stoll, A.M.; Bevirt, J.; Pei, P.P.; Stilson, V.E. Conceptual Design of the Joby S2 Electric VTOL PAV. In Proceedings of the Aviation Technology, Integration and Operations Conference, Atlanta, GA, USA, 16–20 June 2014.

46. Brown, A.; Harris, W. A Vehicle Design and Optimization Model for On-Demand Aviation. In *2018 AIAA/ASCE/AHS/ASC Structures, Structural Dynamics, and Materials Conference*; American Institute of Aeronautics and Astronautics: Kissimmee, FL, USA, 2018. [CrossRef]
47. EVE Air Mobility. Mobility Reimagined. Available online: https://eveairmobility.com (accessed on 9 May 2022).
48. Howard, C.E. Uber Unveils Third eVTOL Common Reference Model Concept for Future Flying Taxis. Available online: https://www.militaryaerospace.com/commercial-aerospace/article/14229631/uber-unveils-third-evtol-common-reference-model-concept-for-future-flying-taxis (accessed on 9 May 2022).
49. AFRPS. *Introduction to V/STOL Technology*; USAF Aerospace Research Pilot School: Edwards, CA, USA, 1970.
50. Lilium. Lilium Jet—The First Electric VTOL (eVTOL) Jet. Available online: https://lilium.com/jet (accessed on 12 November 2022).
51. Joby Aviation. Joby. Available online: https://www.jobyaviation.com (accessed on 12 November 2022).
52. FutureFlight. Neoptera Aero eOpter—Complete Performance Data. Available online: https://www.futureflight.aero/aircraft-program/eopter (accessed on 9 May 2022).
53. Opener Aero. Blackfly. Available online: https://opener.aero (accessed on 12 November 2022).
54. Airbus. A^3 Vahana (1-Seater). Available online: https://acubed.airbus.com/projects/vahana (accessed on 24 December 2019).
55. BETA Technologies. The Future of Flight. Available online: https://www.beta.team (accessed on 12 November 2022).
56. Vertical Aerospace. VX4—Urban Air Mobility—Vertical Aerospace. Available online: https://vertical-aerospace.com/vx4 (accessed on 9 May 2022).
57. Volocopter. Volocopter. Available online: https://www.volocopter.com (accessed on 30 November 2022).
58. Hoversurf. The Idea Is Freedom. Available online: https://www.hoversurf.com/ (accessed on 12 November 2022).
59. Aviation Artur Trendak. T6—Prototype. Available online: https://trendak.eu/pl/modele/t6-prototyp/ (accessed on 12 November 2022).
60. Liu, R.-L.; Zhang, Z.-J.; Jiao, Y.-F.; Yang, C.-H.; Zhang, W.-J. Study on Flight Performance of Propeller-Driven UAV. *Int. J. Aerosp. Eng.* **2019**, *2019*, 6282451. [CrossRef]
61. NASA. *Vehicle Sketch Pad (VSP): Geometric Modeling Software to Support Aircraft Conceptual Design, 3.24.0*; National Aeronautics and Space Administration: Hampton, Virginia, 2021.
62. McDonald, R.A.; Gloudemans, J.R. Open Vehicle Sketch Pad: An Open Source Parametric Geometry and Analysis Tool for Conceptual Aircraft Design. In Proceedings of the AIAA SCITECH 2022 Forum, San Diego, CA, USA, 3–7 January 2022. [CrossRef]
63. Archer, C.L.; Caldeira, K. Global Assessment of High-Altitude Wind Power. *Energies* **2009**, *2*, 307–319. [CrossRef]
64. Stojakovic, P.; Rasuo, B. Single propeller airplane minimal flight speed based upon the lateral maneuver condition. *Aerosp. Sci. Technol.* **2016**, *49*, 239–249. [CrossRef]
65. Stojaković, P.; Velimirović, K.; Rašuo, B. Power optimization of a single propeller airplane take-off run on the basis of lateral maneuver limitations. *Aerosp. Sci. Technol.* **2018**, *72*, 553–563. [CrossRef]
66. Zhao, S.; Guo, Z.; Yan, K.; Wan, S.; He, F.; Sun, B.; Wang, G. Towards high-energy-density lithium-ion batteries: Strategies for developing high-capacity lithium-rich cathode materials. *Energy Storage Mater.* **2021**, *34*, 716–734. [CrossRef]
67. Adu-Gyamfi, B.A.; Good, C. Electric aviation: A review of concepts and enabling technologies. *Transp. Eng.* **2022**, *9*, 100134. [CrossRef]
68. Sholz, D. Empennage sizing with the tail volume complemented with a method for dorsal fin layout. *INCAS Bull.* **2021**, *13*, 149–164. [CrossRef]
69. Chapra, S.C.; Canale, R.P. *Numerical Methods for Engineers*, 2nd ed.; McGraw-Hill: New York, NY, USA, 1990; p. 812.
70. Martins, J.R.R.A.; Ning, A. *Engineering Design Optimization*; Cambridge University Press: Cambridge, UK, 2021. [CrossRef]
71. International Organization for Standardization. ISO 3166—Country Codes. Available online: https://www.iso.org/iso-3166-country-codes.html (accessed on 1 August 2022).
72. Micor Technologies. AMVA. Available online: https://micortec.com (accessed on 12 November 2022).
73. EHang. UAM—Passenger Autonomous Aerial Vehicle (AAV). Available online: https://www.ehang.com/ehangaav (accessed on 12 November 2022).
74. Astro Aerospace. The Future Is Here. Available online: https://flyastro.com (accessed on 12 November 2022).
75. Turkish Technic. Esinti. Available online: https://turkishtechnic.com (accessed on 12 November 2022).
76. Wisk Aero. Autonomous Urban Air Mobility. Available online: https://wisk.aero/aircraft (accessed on 30 November 2022).
77. Flyka Aero. eVTOL Aircraft, Unmanned & Safe. Available online: https://flyka.aero (accessed on 12 November 2022).
78. Lift Aircraft. Hexa eVTOL. Available online: https://www.embention.com/projects/hexa-evtol/ (accessed on 12 November 2022).
79. Limosa. LimoConnect. Available online: https://limosa.ca (accessed on 12 November 2022).
80. Xpeng. Voyager X2. Available online: https://www.aeroht.com (accessed on 12 November 2022).
81. Napoleon Aero. VTOL. Available online: https://iz.ru/677018/sergei-valchenko/taksi-s-vertikalnym-vzletom (accessed on 9 May 2021).
82. EMRAX. EMRAX Electric Motors/Generators. Available online: https://emrax.com/e-motors/ (accessed on 26 September 2022).
83. MAGicALL. Magnetic Components & Electronic Systems—Products. Available online: https://www.magicall.biz/products/ (accessed on 26 September 2022).
84. magniX. Industry-Leading Electric Propulsion Systems. Available online: https://www.magnix.aero/services (accessed on 26 September 2022).

85. Siemens eAircraft. Disrupting the Way You Will Fly! Available online: https://www.ie-net.be/sites/default/files/Siemens%20eAircraft%20-%20Disrupting%20Aircraft%20Propulsion%20-%20OO%20JH%20THO%20-%2020180427.cleaned.pdf (accessed on 26 September 2022).
86. Yuneec. Power Systems. Available online: http://www.yuneec.com/PowerMotor_Tech_spec.html (accessed on 26 September 2022).